Impact of introducing Automatic Transmit Power Control in P-P Fixed Service systems operating in bands above 13 GHz

Ofcom Contract 830000059
Final Report

S.A. Callaghan, I. Inglis, P. Hansell.

Radio Communications Research Unit
CCLRC - Rutherford Appleton Laboratory
Chilton, Didcot
Oxfordshire OX11 0QX
Tel: +44 (0) 1235 445770
Fax: +44 (0) 1235 446140

On behalf of:
CCLRC Rutherford Appleton Laboratory and Aegis Systems Limited.

28th February 2006

Table of Contents

1. SUMMARY 3

2. INTRODUCTION 4

1.1 AIMS OF THE PROJECT 4
1.2 SPECTRUM EFFICIENCY BENEFITS OF INTRODUCING ATPC 4

2. SPATIO-TEMPORAL ANALYSIS AND SIMULATION OF RAIN FIELDS 10

2.1 INTRODUCTION AND RATIONALE 10
2.2 SPATIAL AND TEMPORAL ANALYSIS OF METEOROLOGICAL RADAR DATA 10
2.3 SYNTHETIC RAIN FIELD GENERATOR 20

3. ATPC SYSTEM DEFINITION 32

3.1 ATPC PARAMETERS 33
3.2 SETTING UP THE LINK 33

4. ATPC IMPLEMENTATION TOOL 36

4.1 PLANNING TOOL 36
4.2 ANALYSIS TOOL 45

5. APPLICATION OF ATPC TO OTHER BANDS ABOVE 18 GHZ 56

6. CONCLUSIONS 57

7. REFERENCES 57

APPENDIX 1: SPECTRAL MODELLING OF RANDOM PROCESSES 59

1. Summary

Adaptive transmit power control can be used to improve the spectrum efficiency of fixed links by limiting the transmit power to that required to maintain a constant bit error rate (BER) regardless of the propagation conditions. This results in a reduced transmit power being used during clear sky conditions, meaning that the interference resulting from the ATPC link is correspondingly lower. This improves the frequency reuse factor associated with a given band and geographic area, providing a spectrum efficiency gain.

For systems operating at frequencies of above 10 GHz, the primary propagation impairment is rain. The spatio-temporal distribution of rain fields determines whether interfering links are attenuated in similar proportion to wanted links, thereby indicating if the implementation of ATPC will result in increased levels of interference. To accurately determine this, the spatio-temporal aspects of rain fields were investigated during the project, with the aim of producing a realistic rain field simulator to assist with the analysis of the impact of ATPC.

It was found that the spatial autocorrelation function of rain fields falls off approximately exponentially with distance. A fractal model was used to simulate rain fields. This model is capable of producing stratiform-like and convective-like synthetic rain fields, with fractal dimension of contour lines enclosing areas of rain greater than or equal to a threshold, and a spectral density function exponent and spatial autocorrelation function consistent with measured data.

The project produced two pieces of software:

1. The planning tool, which takes an existing plan and re-plans it, subject to the mix of ATPC and non-ATPC links and the type of ATPC in use. The statistics of the new plan are then calculated to estimate changes in band efficiency.
2. The analysis tool takes a plan generated by the planning tool (or by another process) and applies a sequence of rain fields, evaluating system performance as measured by outage probabilities. For each rain field, the fade on each link is calculated, which then allows the EIRP uplift to be determined for each ATPC link. Every link is then tested in turn against all interfering paths, for all rain fields, and the number of outages recorded (distinguishing between those outages directly caused by a rain fade and those outages caused by ATPC-enhanced interference).

It was found that implementation of ATPC in the 38 GHz band gives significant improvements in spectrum efficiency as measured by the increase in the number of links assigned to channel 1 (from ~50% to ~70%) and the decrease in the maximum bandwidth used (from ~300 MHz to ~180 MHz). The introduction of ATPC does give rise to a number of additional outages in the presence of intense rain (~10% increase for a frontal rain event). Adjusting W/U in the planning process is a more effective technique for reducing ATPC-induced outages than adjusting the fade margins or interference margin. However, it is evident that none of these band-wide mitigation techniques targets the ATPC-induced outages as effectively as a judicious choice of ATPC system parameters.

Based on the similarity of average fade margins between the 38 GHz band and other high frequency fixed link bands, gains in spectrum efficiency should equally be possible in those other bands.

2. Introduction

This document is presented as the final report for the Ofcom contract titled, "Impact of introducing Automatic Transmit Power Control in P-P Fixed Service systems operating in bands above 13 GHz".

1.1 Aims of the project

A previous study funded by Ofcom [Richardson et al, 2004] has indicated that there are spectrum gains to be made as a result of the introduction of ATPC in point-to-point fixed service bands, especially those operating at frequencies where rain is a significant attenuator. However, that study was limited in scope, dealing only with a simplified scenario of two parallel links, separated by distances of ~1–10 km. The previous study raised several questions with respect to the implementation of ATPC in point-to-point fixed services:

1. During rain events, does the use of ATPC increase harmful interference to neighbouring point-to-point systems, exceeding the frequency assignment criteria? And if so, how often and to what extent will the criteria be exceeded?

2. Over what geographical area can rain fading be considered to be correlated? This will have an impact on the worst-case scenarios for the use of all-ATPC and mixed deployments.

3. What is the most efficient way of maximising the increase in packing density and spectrum utilisation through the use of ATPC, without exceeding the assignment criteria?

4. What frequency bands will provide the best results in terms of spectrum utilisation as a result of ATPC implementation, taking into account existing technologies, and inter-service sharing?

These questions form the aims of the project.

1.2 Spectrum Efficiency Benefits of Introducing ATPC

The potential advantages of ATPC reported in the literature include:

- Reduced average power consumption.
- Extended equipment mean time between failure (MTBF).
- Elimination of the 'upfade' problem in receivers.
- Improved outage performance due to the reduced influence of adjacent channel interference (ACI).
- Easier frequency co-ordination in areas of high radio-relay station density.

It is this last point that is fundamental to the objectives of this study, since an increase in spectrum utilisation is dependent on the ability to reduce the co-ordination distance for systems employing ATPC without compromising the quality of service of neighbouring links through excessive interference.

However, it is vital to emphasise that ATPC should only be used to combat temporary fading of the wanted link rather than interference from the unwanted link(s). Otherwise, a situation could arise where two ATPC systems repeatedly increase their Tx power in response to each other's interference until both are transmitting at their maximum Tx power. This situation would reduce

to the non-ATPC case, completely negating any spectrum efficiency benefits gained as a result of employing ATPC in the first place. To avoid this situation, ATPC links must be designed and deployed correctly to take into account the interference generated by neighbouring links so that ATPC is used to combat rain fading, rather than interference.

The US administrations (National Spectrum Managers Association, NSMA) already permit a co-ordination advantage to be claimed for links operating at frequencies below 12.2 GHz [National Spectrum Managers Association Working Group 18 Recommendation on Adaptive Power Control (WG18-91-032)]. The general approach is to follow the standard frequency assignment and co-ordination process defined in the Handbook on Digital Radio-Relay Systems [ITU-R, 1996], but to claim a co-ordination advantage on the basis of a reduced $Tx_{co\text{-}ord}$ Power. This advantage can be claimed if the following conditions are met:

i) the wanted and unwanted paths are de-correlated,
ii) the link with ATPC is at Tx_{max} Power for less than 0.01 % of the time.

This study investigates whether these conditions hold true at higher frequencies, where rain attenuation is the primary fading mechanism. Richardson et al [2004] have already investigated this for a simplified case of two parallel links operating in the 18 GHz band. This study expands on that work to cover large numbers of links in a wider geographical area in the 38 GHz band and briefly investigates the application of ATPC in other bands.

1.2.1 Application of Adaptive Power Control Techniques in Congested Spectrum

The assignment criteria used by Ofcom to determine whether a new frequency assignment can be made to a point-to-point link without receiving or generating unacceptable interference address two different situations:

- The wanted path is in its faded state (i.e. at the Receiver Sensitivity Level, RSL[*]) and the interfering path is in a state that gives rise to its median received signal level, as modelled using ITU-R Recommendation 452.
- The wanted path is in an unfaded state, as represented by the median received signal level[*], and the interfering path is enhanced, once again as modelled using ITU-R Recommendation 452.

In both of these situations it is necessary to satisfy a given wanted to unwanted signal ratio (W/U). Co-channel W/U values may be calculated from first principles and are based on a noise limited frequency assignment methodology where aggregate interference and individual sources of interference are limited to specified levels below an allowance for receiver noise. In practice, at the present time, co-channel and first adjacent channel values are taken from ETSI Standards and modified in order to take account of multiple interferers (this approach is under review and a return to calculation from first principles is envisaged). Offset W/U values, beyond the first adjacent channel, are based on the co-channel value, the Net Filter Discrimination (NFD) associated with the relative bandwidths of the wanted and unwanted signals, the out of band emissions of the interfering signal (transmit mask), the out of band discrimination of the receiver (receive mask) and the frequency offset of the two signals.
The implications of ATPC for this assignment process are shown in the following schematics. It should be noted that these schematics do not show all of the complexities. For example, outages are treated as instantaneous at peak fade or enhancement points—outage times are therefore not completely represented. Also, the schematics are not meant to be to scale, but it

[*] These values are known a priori and the relationship between them is the margin (M) as calculated using ITU-R Recommendation 530.

can be assumed that the power increase during a fade on the unwanted link gives rise to no more interfering power than the baseline case (i.e. no ATPC).

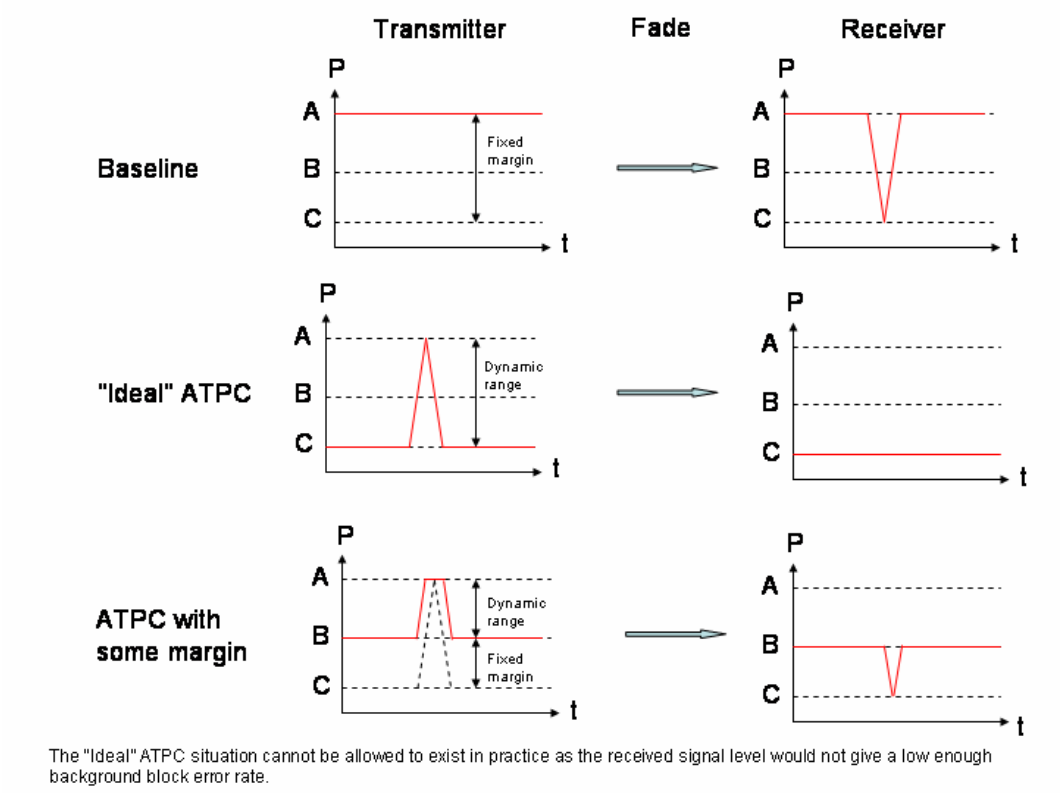

Figure 1: Schematic examples of the power against time for the transmitter and receivers in a non-ATPC system, an ideal ATPC system and an ATPC system with some margin.

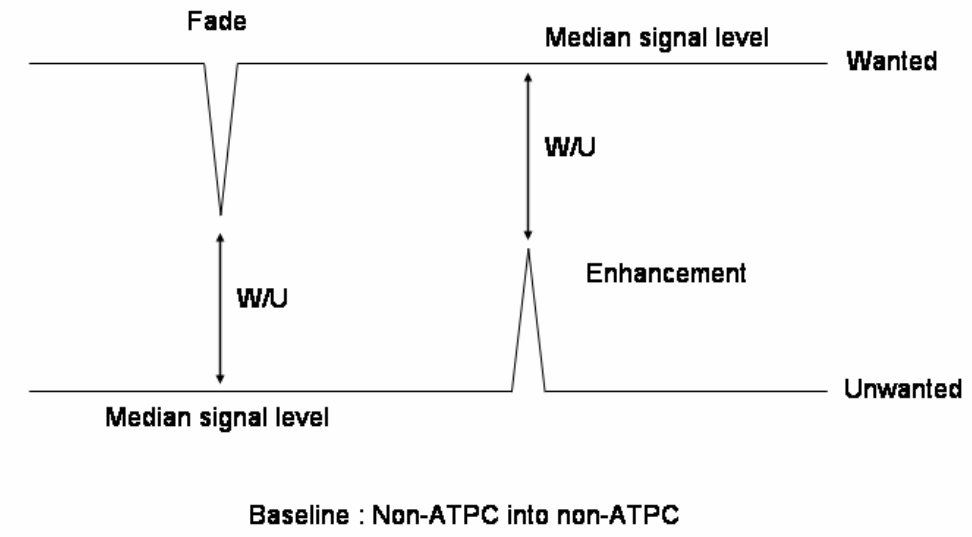

Figure 2: Schematic example of the W/U for a non-ATPC system interfering with another non-ATPC system (baseline case)

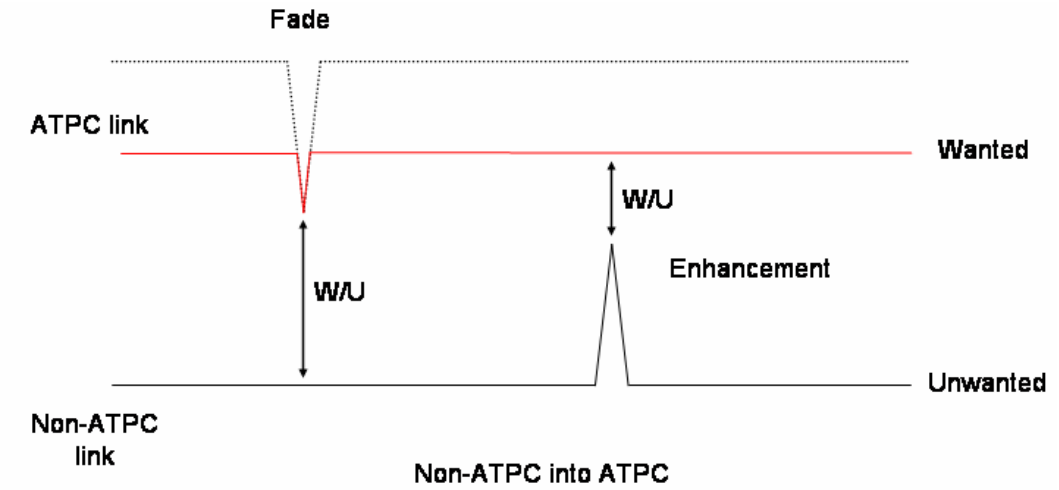

Figure 3: Schematic example of the W/U for a non-ATPC system interfering with an ATPC system

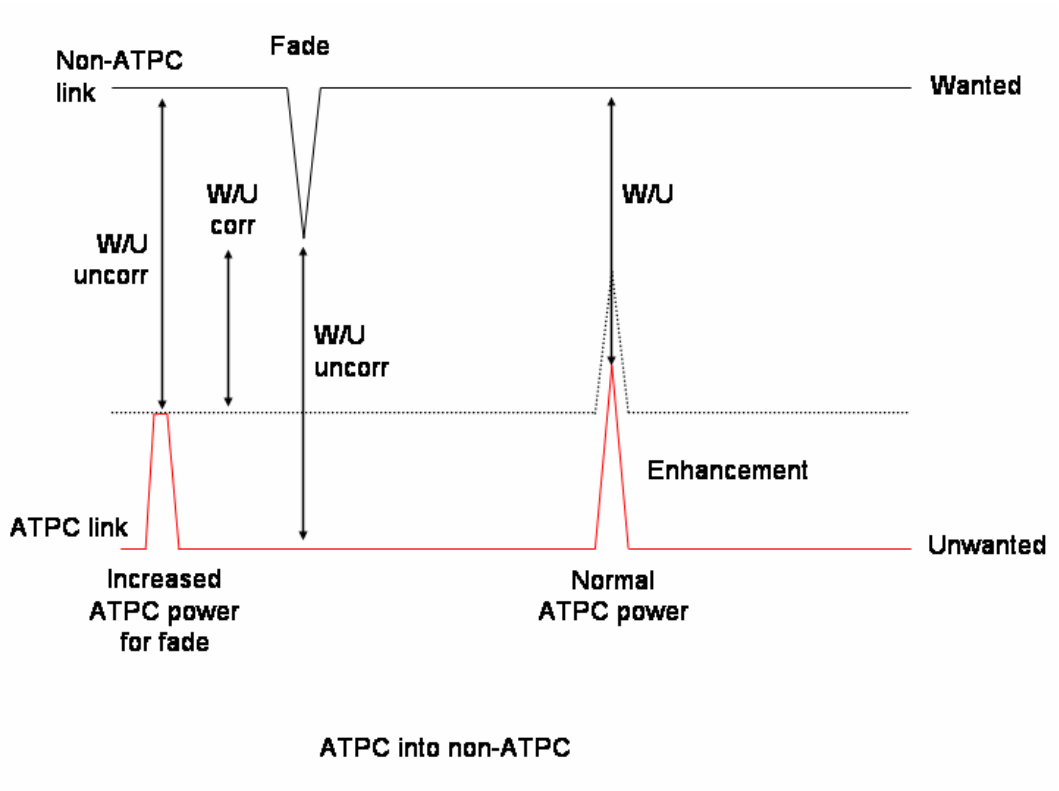

Figure 4: Schematic example of the W/U for an ATPC system interfering with a non-ATPC system

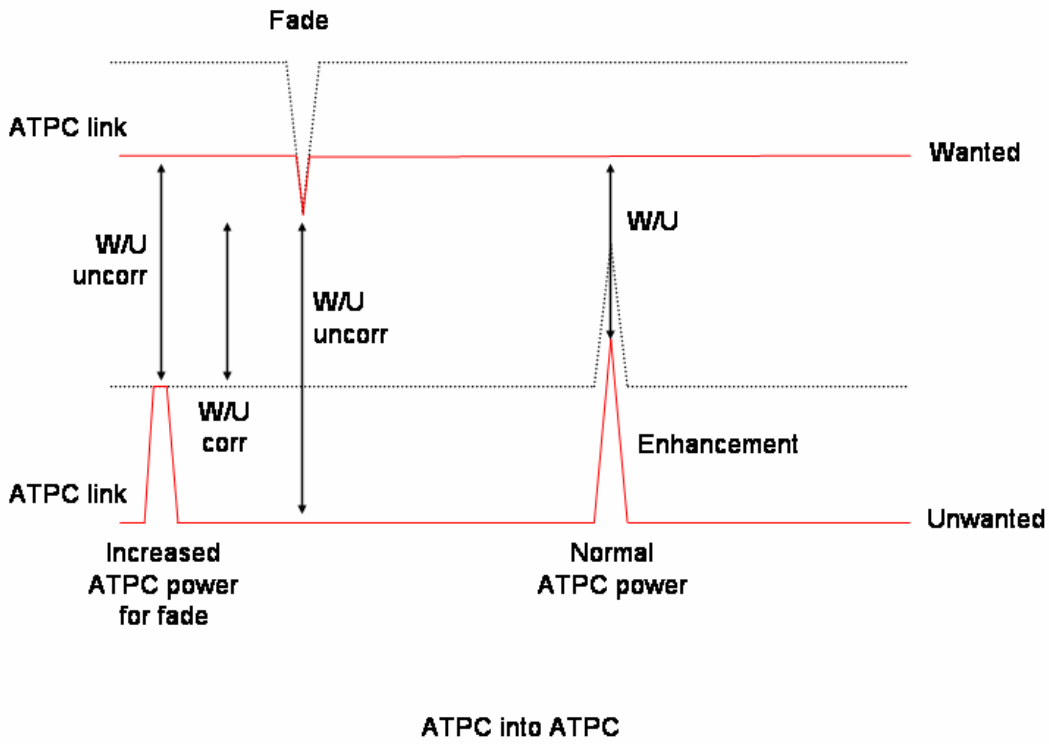

Figure 5: Schematic example of the W/U for an ATPC system interfering with an ATPC system

	Impact of power changes arising from ATPC		Impact of unwanted enhancements
Mixed: Non-ATPC into ATPC	Same as baseline		Worse than baseline
Mixed: ATPC into non-ATPC	Better than baseline	Same as baseline	Better than baseline
All ATPC	Better than baseline	Same as baseline	Better or worse than baseline depending on the relative dynamic ranges on the wanted and unwanted links[1].
	Uncorrelated	**Correlated**	

Table 1: Comparison with respect to the baseline case (i.e. non-ATPC into non-ATPC)

The correlation referred to above is with respect to the fade (due to rain) on the wanted link and the unwanted link.

The situation is more complicated than the simplified schematics above because there will probably be rain attenuation on the interfering path itself—this is not represented in the diagrams.

[1] If all dynamic ranges were to be the same then this situation would be the same as the baseline.

In terms of modelling the effect of ATPC combating rain fades on the assignment process, it is clear that some account has to be taken of unwanted enhancements as these are reflected in one of the criteria used in the assignment process. It can be seen from the table above that it is potentially the enhancements that cause a problem when mixed deployments (non-ATPC and ATPC) are allowed.

We need to consider whether ATPC can also combat this effect by increasing the wanted power level. However, it should be noted that this can only be done in response to a degradation in BER and not in the received signal level as this will effectively be constant. Earlier comments regarding the "domino effect" that could occur when using BER as the fade detection mechanism need to be taken into account.

1.2.2 Co-ordination Issues

The primary co-ordination issues associated with the 38 GHz band are intra-service ones, i.e. this band is solely shared by fixed terrestrial services. However, there are higher frequency bands where fixed terrestrial links share with fixed satellite services, and the implications of this should be investigated in future work.

1.2.3 Interference Management Techniques

It is not clear how the outage allowance (e.g. 0.01% time when the availability requirement is 99.99%) is attributed to the fade in the absence of interference, the presence of "median" interference and the presence of "enhanced interference".

Fade Margin (no interference) is calculated on the basis of the rainfall rate for 0.01% of the average year.

In the presence of "median" interference during a fade the C/(N+I) will decrease—an allowance of 1 dB is made for interference and this is apportioned to multiple entries. As long as the interference stays within the W/U limits there is no impact on the outage allowance.

The "enhanced" interference is calculated from ITU-R Recommendation 452 on the basis of the required time percentage(s) for which the calculated basic transmission loss is not exceeded.

1. If it were to be assumed that there are n "enhanced" interference entries then the outage would be 0.01% (fade) + n x 0.01% ("enhanced") interference.

2. It might be argued that one or other mechanism dominates (i.e. one or other of the two criteria determines whether an assignment can be made, but not both) and if the interference margin is not fully used (by median interference) the fade outage time will be slightly less. This still leaves the possibility of n x 0.01% outage attributable to the "enhanced" interferers.

3. However, the W/U ratio required for each entry has been adjusted (in power terms) to reflect multiple entries and there is a 1 dB allowance for interference. This power difference will be reflected by shorter outages for each entry so it becomes n x <0.01%.

4. It might be further argued that the likelihood of all "enhanced" entries being the same is very small in which case the tendency is back towards all "enhanced" entries giving rise to 0.01% outage.

As can be seen, interference management is a key part of assessing the gains to be made from ATPC implementation.

2. Spatio-temporal analysis and simulation of rain fields

2.1 Introduction and rationale

The primary and most important output of this project is a working and realistic system planning tool. ATPC is envisaged as a tool to combat rain fading, hence in order to optimise its use, a thorough understanding of rain and how it impacts on terrestrial links is required. As there is currently limited measured rain data available to apply to the analysis tool, it is necessary to use the most advanced rain model possible in the simulator. This provokes a need to investigate the spatial and temporal behaviour of rain fields at a time and space resolution appropriate to the link lengths being investigated.

A potential source of radar rain fields for systems designers in the UK is the Met Office's Nimrod database. Available from the British Atmospheric Data Centre (BADC—http://www.badc.rl.ac.uk), Nimrod is a fully automated system for weather analysis and nowcasting based around a network of C-band (4–8 GHz) rainfall radars. The BADC holds the analyses at a time resolution of 15 minutes, along with composite pictures of the rain rate as measured by the radar network. Composite rain radar data on the Cartesian national grid are available from late 2002, and files are updated on a regular basis. From April 2004, data is available on a time resolution of 5 minutes, and with a hybrid space resolution of 1/2/5 km. However, even these higher resolutions are not sufficient to accurately characterise the fast fluctuations in rain events that can impact heavily on systems using ATPC.

2.2 Spatial and temporal analysis of meteorological radar data

2.2.1 Data description

The rainfall rate contours analysed in this research have been obtained by means of the Chilbolton Advanced Meteorological Radar (CAMRa), which is located in Hampshire in the south of England, at the latitude 51˚ 9' North and the longitude 1˚ 26' West. The climate is temperate maritime, with an average annual rain rate exceeded for 0.01% of the time of approximately 22.5 mm/hr. The radar is a 25 m steerable antenna, equipped with a 3 GHz Doppler-Polarization radar, and has an operational range of 100 km, and a beam width of 0.25˚. To avoid reflections from ground clutter, maps of the rain rate field near the ground were produced by scanning with an inclination of 1.2˚. These maps are produced on a polar grid, with a range resolution of 300 m and an angular resolution of 0.3˚. The number of maps produced in a given time period is dependent on the total angle scanned. The radar has a maximum angular velocity of 1˚/second.

The radar scans were interpolated onto a square Cartesian grid, with a grid spacing of 300 m and a side length of 56.4 km. Each grid contains 35344 data points (188^2) covering more than 3100 km². The grids are separated in time by approximately 2 minutes.

2.2.2 Spatial autocorrelation

It can be assumed that the spatial correlation of rain falls off exponentially with distance for the first 50 km or so [Paraboni et al, 1998, Richardson et al, 2004]. The de-correlation for rain rate for large distances (up to 1000 km) and multiple stations was presented by Barbalisica et al, [1992], using a very large rain gauge database covering the entire Italian territory. They have shown that for distances greater than 50 km the fall-off of spatial correlation with distance slows, though there can be jumps due to a recoupling effect resulting from the presence of

another separate rainy event occurring at far distances at the same time. For their data, it was reported that statistical independence was reached for distances between sites greater than 800 km.

Figures 6a, 6b and 6c show the two-dimensional spatial autocorrelation function calculated for three different types of event measured by CAMRa, convective, frontal and stratiform respectively. As can be seen, the correlation coefficient falls off quickly with distance in all three cases, approaching zero for distances of around 180 pixels (corresponding to 54 km). This agrees well with the general assumption mentioned above.

A key point is the differences in behaviour of the autocorrelation function for the different event types. As can be seen, the autocorrelation function for the convective event falls off more quickly with distance than the autocorrelation function for the stratiform event. The autocorrelation function for the frontal event appears as a mixture between the two others. This is due to the phenomenological behaviour of the different types of rain event.

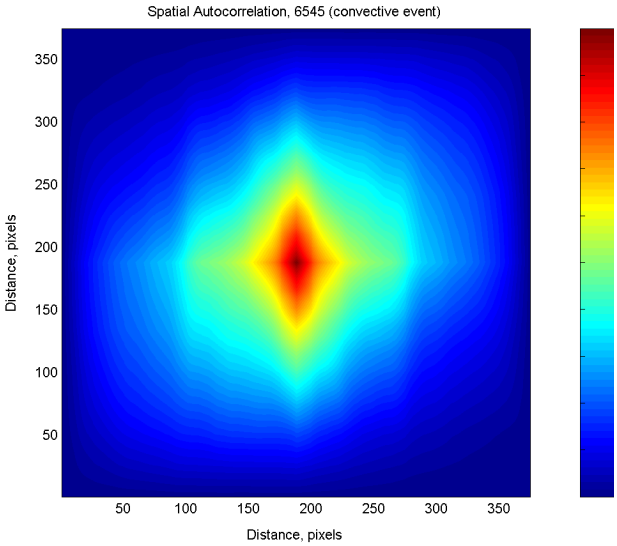

Figure 6a: Spatial autocorrelation for a convective event

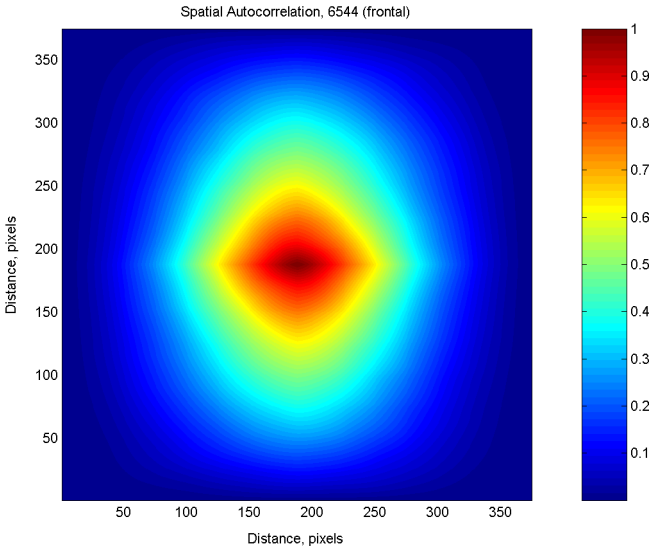

Figure 6b: Spatial autocorrelation for a frontal event

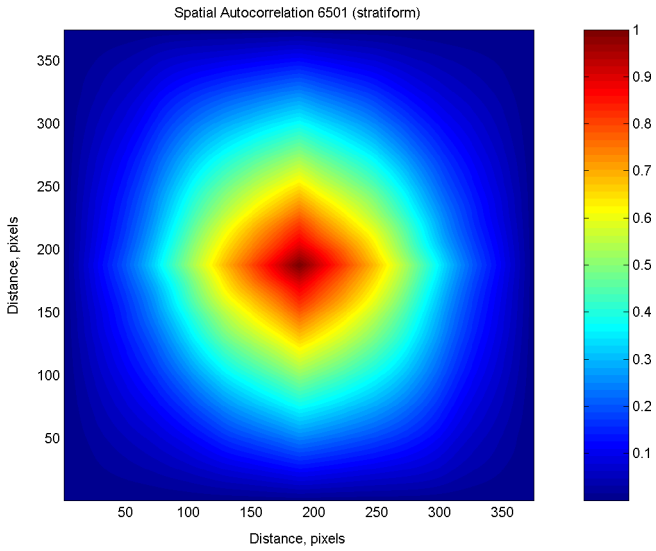

Figure 6c: Spatial autocorrelation for a stratiform event

A better view of the fall-off of spatial correlation with distance can be seen in figures 7a, 7b and 7c. In these figures, radial cross-sections have been taken from the centre points of the auto-correlation plots at different angles to the edges.

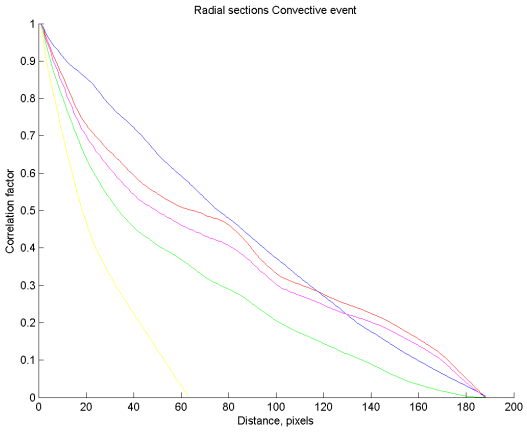

Figure 7a: Radial sections through the spatial autocorrelation for a convective event

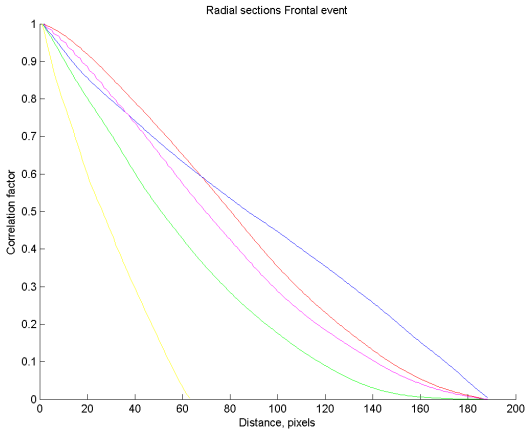

Figure 7b: Radial sections through the spatial autocorrelation for a frontal event

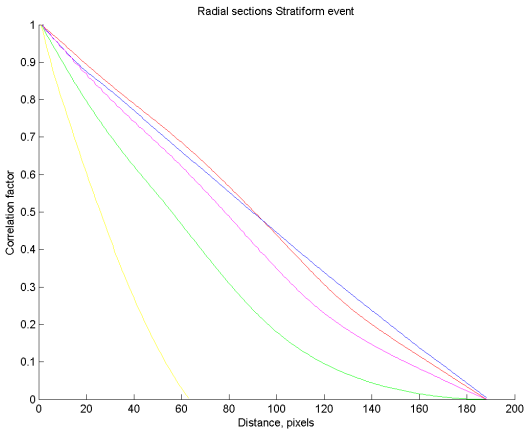

Figure 7c: Radial sections through the spatial autocorrelation for a stratiform event

These figures show that the fall-off of autocorrelation coefficient with distance can be approximated by an exponential decay, as described in the literature, though as shown before, the rate of that decay is steeper in the convective rain fields than in the stratiform and frontal fields.

2.2.3 Cross-correlation between measured radar rain fields

The autocorrelation function looks purely at the rain fields in terms of the difference between points separated in space, while the cross-correlation investigates the relationship between points separated in time and space.

The normalised two-dimensional cross-correlation can be obtained between two radar snapshots (also known as rasters) using the following equation:

$$\rho(R_1 R_2) = \frac{\Gamma(R_1 R_2)}{\sqrt{\max(\Gamma(R_1))} * \sqrt{\max(\Gamma(R_2))}} \quad (1)$$

where:

$\Gamma(R_1 R_2)$ is the covariance function obtained from the expression:

$$\Gamma(R_1 R_2) = < (R_1 - m_1)(R_2 - m_2) > \quad (2)$$

$R_1 = R(x, y, t = t_1)$, the rain field at time t_1

$R_2 = R(x, y, t = t_2)$, the rain field at time t_2

and m_1, m_2 are the mean values of the field R_1 and R_2 respectively.

Figures 8a, 8b and 8c show the normalised cross-correlation between two rasters (snapshots) of each rain event, separated in time by 10 rasters (approximately 20 minutes). This time separation was chosen as it is assumed that significant evolution of the rain fields will not have occurred during this time, even though the rain field has moved across the scan area, i.e. that the frozen field hypothesis [Taylor, 1938] holds for this time separation [2].

The patterns for the different rain events are quite revealing. The stratiform event has a cross-correlation that has a very broad, almost elliptical, base, indicating that the event itself is widespread with little variation. The convective event has a series of low, but quite sharp peaks, indicating the more cell-like structure of convective rain. And the frontal event seems to be a mixture of the two, which is not surprising given the nature of the event itself (a band of stratiform rain studded with convective cells).

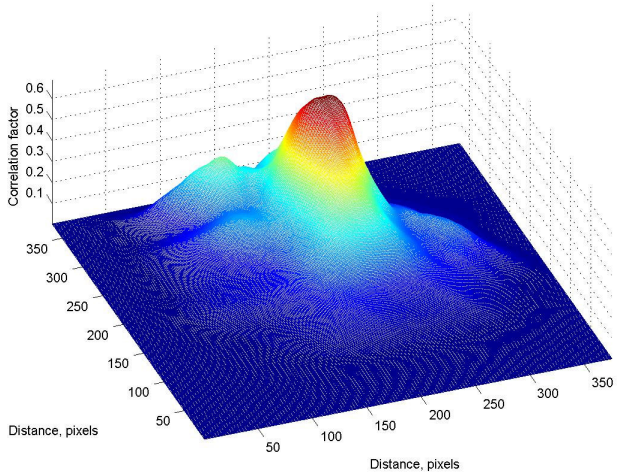

Figure 8a: Normalised cross-correlation function for stratiform event recorded 7th December 2000. 1 pixel corresponds to an area of 300 m * 300 m.

[2] The frozen field hypothesis [Taylor, 1938] postulates the equivalence between the spatial autocorrelation at a fixed point in time and the temporal autocorrelation at a fixed position in space. For this to hold, the spatial argument of the former must be interpreted as a time lag of the latter and the spatio-temporal field must be a fixed spatial field moving with a constant velocity. It has been shown [Zawadski, 1973] that this holds approximately for time lags under about 40 minutes.

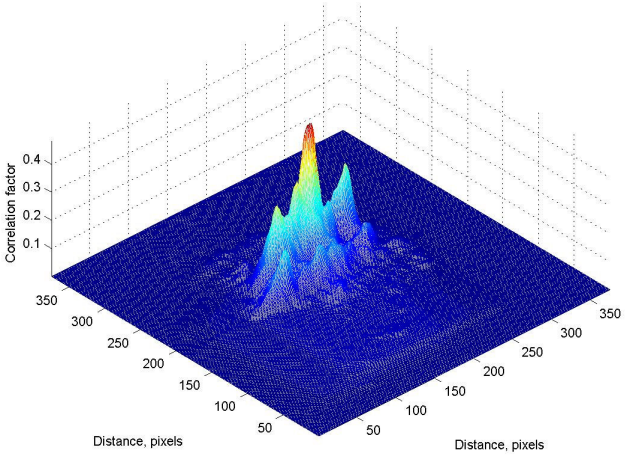

Figure 8b: Normalised cross-correlation function for convective event recorded 16th May 2001. 1 pixel corresponds to an area of 300 m * 300 m.

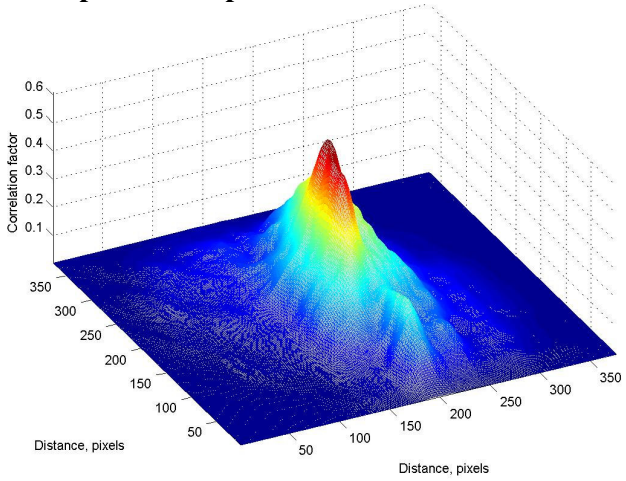

Figure 8c: Normalised cross-correlation function for frontal event recorded 1st May 2001. 1 pixel corresponds to an area of 300 m * 300 m.

2.2.4 Statistics of rain cell sizes

Figures 9 and 10 show the distribution of the number of contour lines that enclose an area greater than or equal to a specific area threshold. As can be seen, the vast majority of contour lines enclose areas of less than 10 km². As the rain rate threshold enclosed by the contour lines increases, there is a corresponding decrease in the absolute number of contours recorded at that threshold. However, when the numbers of contours are normalised to reflect percentage of the total number of contours at that rain rate threshold, for areas less than ~50 km² there is little difference in the area distribution curves for the different rain rate thresholds. Above ~50 km² the spread in the curves widens dramatically, due to climatological reasons. It is well known that the more intense (convective) rain cells are limited in space and occur less often than rain at lower thresholds.

These plots confirm the commonly held opinion that rain cells tend to have dimensions of the order of 1 to 10 km.

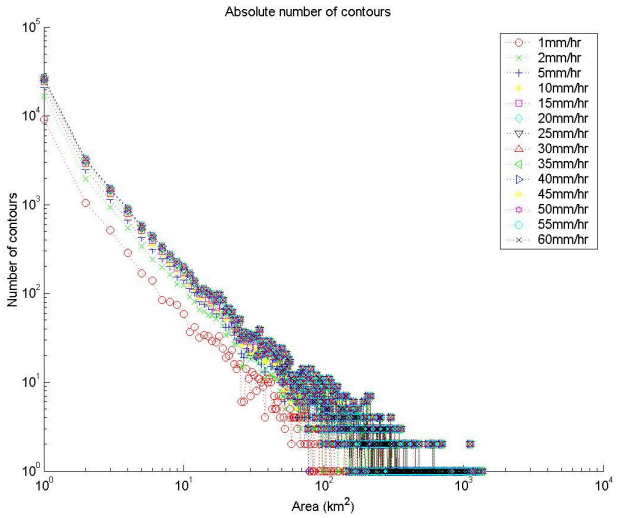

Figure 9: Absolute number of contours greater than or equal to a specific area, calculated for differing rain rate thresholds.

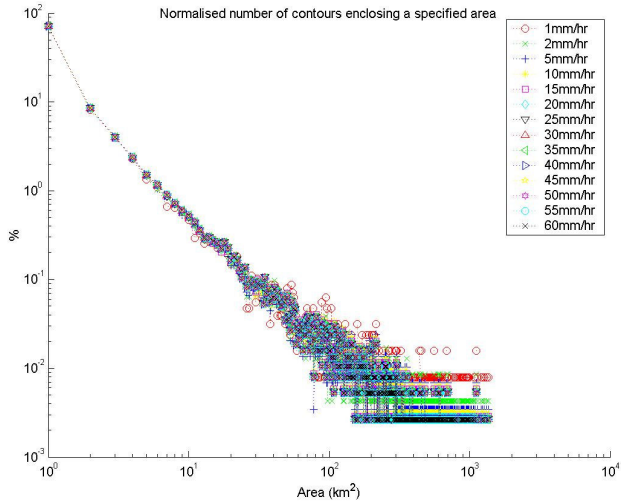

Figure 10: Normalised number of contours greater than or equal to a specific area, calculated for differing rain rate thresholds.

2.2.5 Two-dimensional FFT

If each near-horizontal radar scan is treated as an instantaneous snapshot of the rain rate field then the spatial spectral density may be calculated via 2-D Fourier transform. Figure 11 illustrates the two-sided spectral density of spatial (log) rain rate variation, averaged over the 230 scans recorded for the event that occurred on the 1st May 2001. The near circular contours are consistent with a rotationally symmetric, and hence quadrant symmetric, spectral density and spatial autocorrelation. This shows that the (log) rain field is isotropic, i.e. that there is no preferred direction or spatial scale. The units of 1/km define the spatial frequency.

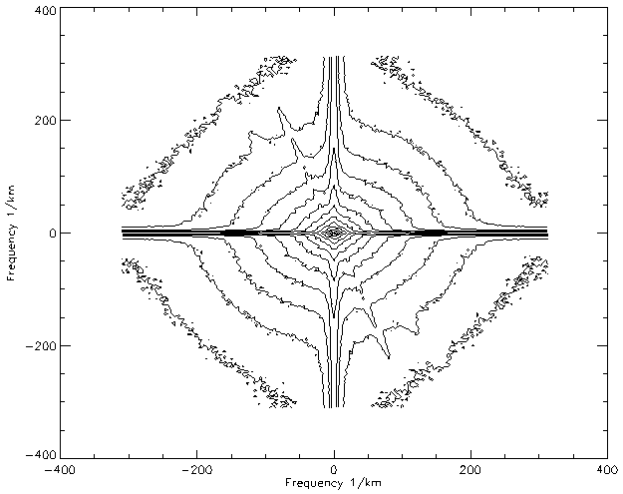

Figure 11: 2-D Spatial spectral density of rain rate for event on 1st May 2001, averaged over 230 scans.

Figures 12a and 12b show the corresponding spatio-temporal isocorrelation contours in the Fourier space for the x-t and y-t sections respectively. We can see from these that the contours have undergone a rotation from the circularly symmetric as a result of the general overall advection present during the event. Empirically observed "squashing" of the contour lines by the wind could also be partially responsible for the change from circular contours to elliptical ones in the 2-D FFT. In figure 11, the cross in the centre of the graph is due to the edge effects of the 2-D FFT; a discontinuity is created at the edges where a tiling is performed in order to turn the discrete sample into a continuous function suitable for analysis. In figures 12a and 12b this edge effect is only seen in the space direction (along the y axis), as there were more samples recorded in time, and there was less of a discontinuity in the time samples.

In figures 11, 12a and 12b the contours have been shifted so that the centre of the figure is the origin. Similar results are presented in [Marsan et al. 1996].

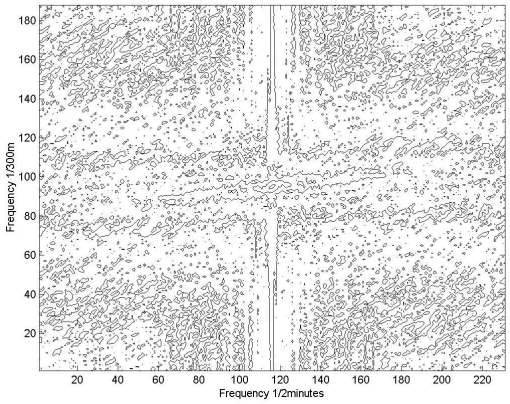

Figure 12a. 2-D Spatial-temporal (x-t) spectral density of rain rate for event on 1st May 2001, averaged across the y direction.

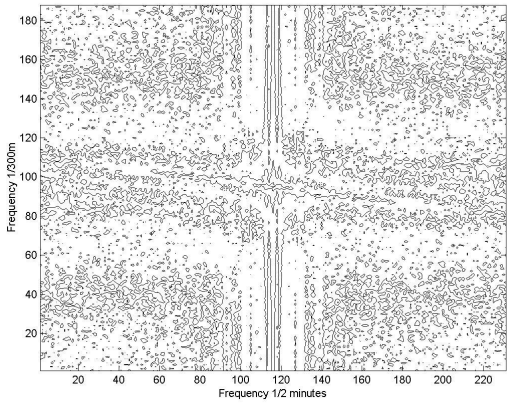

Figure 12b. 2-D Spatial-temporal (y-t) spectral density of rain rate for event on 1st May 2001, averaged across the x direction.

The spectral density function for a two dimensional isotropic random field is given by:

$$S(\omega) \propto \omega^{-2H-2} \tag{3}$$

where H is the Hurst exponent, and is equal to 1/3. For surfaces, the fractal dimension D is related to the Hurst exponent by $D_{surface} = 3 - H$ and $D_{boundary} = D_{surface} - 1$, where $D_{surface}$ is the fractal dimension of the surface and $D_{boundary}$ is the fractal dimension of a contour line drawn on the surface.

Figure 13 shows the averaged radial spectral density of the log rain rate recorded during the event. As can be seen, it is a straight line with a slope = –2.79. Table 2 gives the spectral density exponent calculated for the three different types of events studied. The theory [Kraichnan and Montgomery 1980] predicts a slope of –8/3 (–2.66) in certain regions of the power spectrum. Our results are consistent with this, even though they tend to overestimate slightly.

The unit of spectral density, km, is derived as follows. The rain rate we use in analysis is rain rate relative to 1 mm/hr, which changes our rain rate into a dimensionless unit.

$$spectral\ density = (power)^2 \ / \ frequency \tag{4}$$

where the relative rain rate is equivalent to power. A dimensionless unit squared is still dimensionless, giving the spectral density unit = 1/frequency = 1/(1/km) = km.

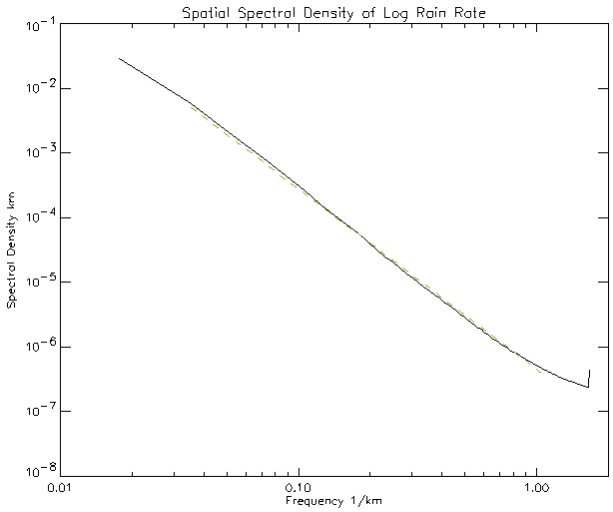

Figure 13. Spectral density of log rain rate for event on 1st May 2001. Exponent = –2.79

Rain event date and type	Radial Spectral Density Exponent
1st May 2001 Frontal event	–2.79
7th December 2001 Stratiform event	–2.89
16th May 2001 Convective event	–2.91

Table 2: Radial spectral density exponent calculated for a frontal, stratiform and convective event at different rain rate thresholds.

2.2.6 Event types and their impact

As can be seen from the investigation of the spatial autocorrelation and cross correlation of the measured radar rain fields, there is a difference in the statistical behaviour of the rain fields according to the event type. This leads us to study the phenomenological aspects of the rain types.

For this reason, we first of all consider figure 14, which is an example raster from a stratiform rain event recorded on the 7th December 2001. A number of key features can be seen immediately:

1. The rain is spread out over a large geographical area (confirmed by the autocorrelation and cross-correlation functions plotted earlier).
2. The rain is of low overall intensity, with a peak value of 7 mm/hr in this case.
3. There are few neighbouring "islands" of rain; most of the rain is gathered in the same large area.

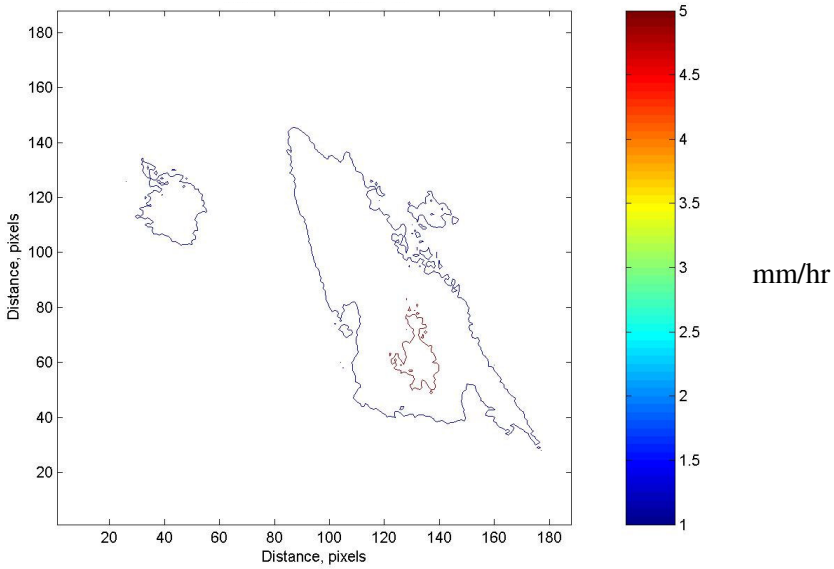

Figure 14 Example raster from the stratiform rain event recorded on the 7th December 2000. Contour lines are drawn at 1 and 5 mm/hr (1 pixel corresponds to an area of 300 m * 300 m)

Similarly, an example of a convective rain field is shown in figure 15. It was recorded on the 16th of May 2001, and demonstrates key features of a convective rain field:

1. The areas of rain cover smaller geographical areas than those in a stratiform event. (This is confirmed by the autocorrelation and cross-correlation functions plotted earlier.)
2. Unsurprisingly, the rain in those smaller areas (commonly known as "rain cells") is quite intense, with peak values of up to 40 mm/hr in this case.
3. The rain is not limited to one or two locations, but instead there are a sizeable number of cells, though some have merged to form a larger cell with two or more peaks. If we look at the field in terms of the total area covered by rain, that area is not condensed into one large widespread area, but instead is fragmented, with gaps between the rain cells.

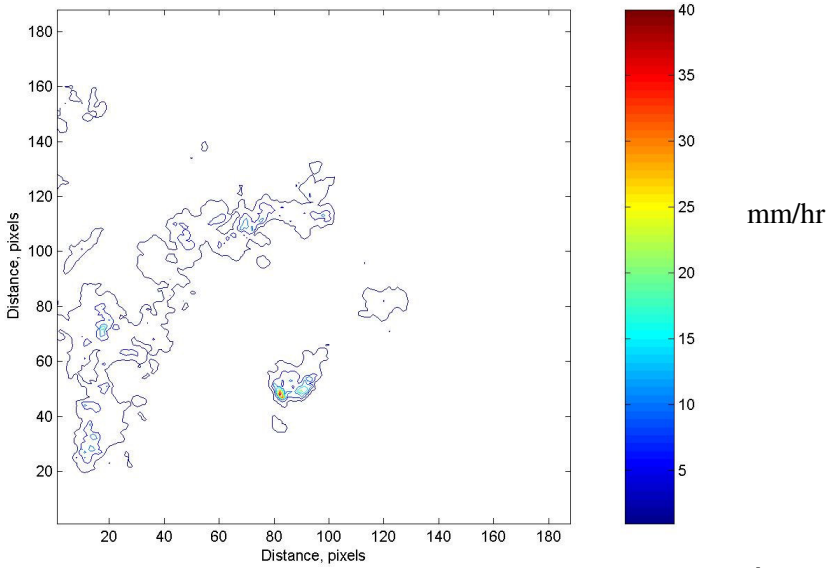

Figure 15 Example raster from the convective rain event recorded on the 16th May 2001. Contour lines are drawn at 1, 5, 10, 15, 20, 25, 30, 35 and 40 mm/hr (1 pixel corresponds to an area of 300 m * 300 m)

2.2.7 Impact of wind on rain rate contours

The data set recorded on the 1st May 2001 was that of a strong frontal event. Therefore the wind direction was remarkably constant over the period the radar was scanning. Figure 16 shows an example of the contour lines recorded for one scan during that event. The snapshot presented in figure 16 is part of a wider radar scan, which took 80 seconds to complete. Hence it can be considered to be a near-instantaneous snapshot of the rain field.

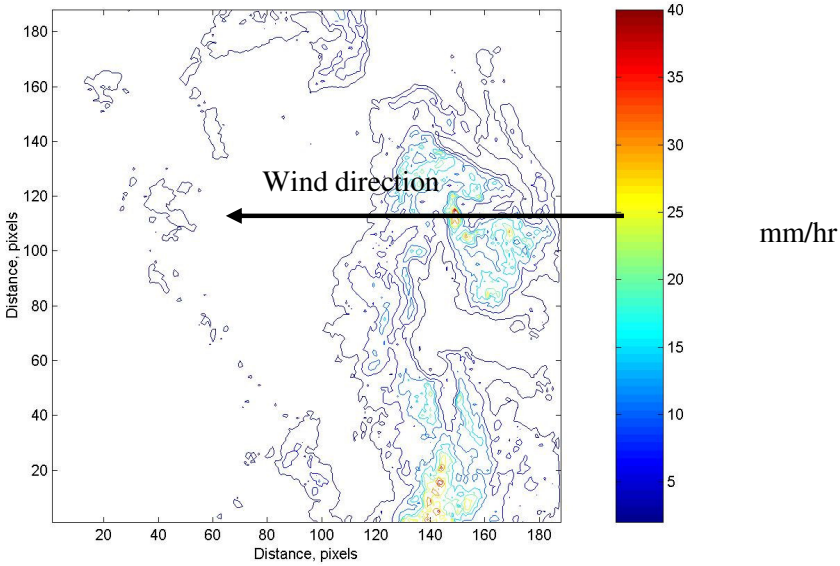

Figure 16: Example of the contour lines produced for one scan recorded on the 1st May 2001. Contour lines are at values of 1, 5, 10, 15, 20, 25, 30, 35 and 40 mm/hr

The wind direction recorded at Chilbolton during the event shown in figure 16 was due North. Because of the way the radar data was mapped onto a Cartesian plane, this translates as the wind blowing along the direction of the negative x-axis. The average wind speed recorded at Chilbolton during this frontal event was approximately 8 m/s, with maximum gusts of 15 m/s.

It appears that the wind "compresses" the rain cells along the line parallel to the direction of the wind, and the rain cells are elongated along a line perpendicular to the direction of the wind. At this time there do not seem to be any studies in the literature that investigate whether or not the amount of compression and elongation is related to the wind speed.

2.3 Synthetic rain field generator

2.3.1 Model requirements

According to Bacon [Rainmap presentation, 2005], a physically based rain model should:

- Have a time resolution of 1 second
- Have a spatial resolution of about 100 m
- Be able to take inputs from a weather model
- Be suitable for use in spectrum management and simulation software

Of those points, the fourth is the easiest to address, as the work on the simulation software was carried out in parallel with the work on the rain model used on the simulator, so the two complement each other. The other three points are addressed later, during the description of the rain field simulator used in this project.

2.3.2 Previous models

Figure 17 shows a summary of the main methods for simulating rain fields discussed in the literature. As can be seen, there are three main areas, discrete cascades, synthetic storms and random space-time function generators (also known as continuous cascades). What follows is a brief discussion and review of these three methods.

Synthetic storm models [Cowpertwait, 1995, Cox and Isham, 1988, Wheater et al, 2000] do not take into account the scaling nature of rain, instead choosing to model storms through the use of stochastic models of physical processes such as: probability distributions and parameters of storm interarrival and duration, rain cell interarrival and duration, correlation structure, point intensity distributions etc. The resulting models describe the arrival and movement of storms and rain cells, but require large numbers of parameters.

Continuous cascades make use of generators of random space-time functions to generate fields with specified spatial and temporal covariance structures. Examples of such cascades are given in [Gremont, 2002, Paulson, 2002 Tessier et al., 1993]. These models are quite flexible, and can incorporate constraints to observed values at appropriate positions. But they also require detailed specifications of the correlation structure of the random function in both space and time, which can be hard to define, and as yet no consensus has been reached on the general structure. Work is currently in progress on the correlation structure of rain fields at the microscale level [Enjamio, 2002], which may help rectify this situation.

The Voss algorithm [Voss, 1985] for discrete cascades is the basis of the rain field simulator used in this project and will be described in detail in the following section. Other discrete cascade models are described in [Deidda, 1999, Over and Gupta, 1996]. The iterative process involved in creating a discrete cascade follows the same basic steps. Start with an isotropic area and divide it into a number of segments. For each segment, a value is assigned which takes into account the value of the area at the previous step, of which it was a part, and scaled according to the step number, with some randomness added by means of addition or multiplication by a random variable with a set probability distribution. This process is then repeated, subdividing further until the required level of resolution is reached.

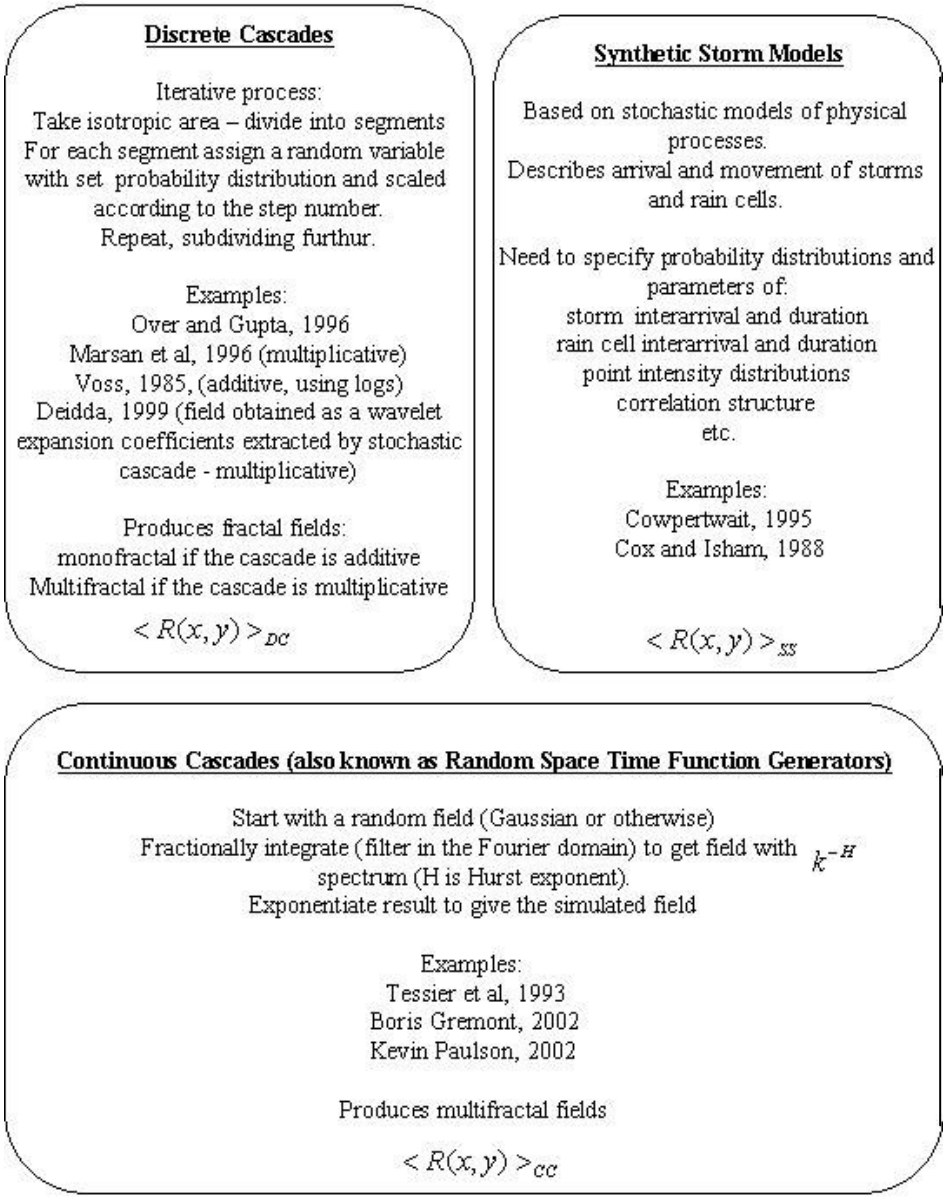

Figure 17: Description of the three main types of procedure used to model the spatial distribution of rain

Discrete cascades exploit self-affinity and self-similarity relationships to produce rain rate fields through an iterative random cascade procedure. These cascades are better able to incorporate non-rainy regions than continuous cascades, and have concepts and ideas in common with disaggregation and downscaling studies [3] done in hydrology [Onof et al., 1996, Charles et al, 1999, Koutsoyiannis and Onof, 2001]. On the other hand it is more difficult to describe the temporal evolution of rain fields using discrete cascades, though it is by no means impossible.

[3] Disaggregation and downscaling involve taking rain data at coarse resolutions (for example, rain gauge time series recorded at daily intervals) and process them to provide realisations at higher resolutions (e.g. producing rain gauge time series at hourly intervals from the daily time series). Downscaling indicates that the resulting realisations are only restricted by the required statistics, while in disaggregation, the resulting realisations must have the required statistics as well as adding up to the observed high resolution data (i.e. hourly rate).

Over and Gupta [1996] demonstrate a method of calculating a discrete random cascade, which distributes mass on successive sub-divisions of a *d*-dimensional cube, to which independent and identically distributed (iid) random variables called generators are applied. This theory is expanded from space to space-time by replacing the iid generators W, with iid stochastic processes $\{W_t, t > 0\}$.

Both types of cascade model are more algorithmic schemes for generating space-time fields than attempts to provide a valid physical representation of a rain event within a given framework. It is for this reason that model parameters were introduced into the simulator presented here, which relate to observed climatological parameters.

2.3.3 Description of the rain field simulator

To simulate the rain field we contemplate the use of the successive random addition algorithm introduced by Voss [Voss, 1985] to generate fractional Brownian motion. The algorithm is easily extended to higher dimensions and can produce surfaces with coastlines that are self similar fractals with a fractal dimension given by:

$$D = 2 - H \tag{5}$$

H is the so-called Hurst exponent, and is related to the power spectral density exponent of the measured rain fields. The spectral density function for a two-dimensional isotropic random field is given by [Paulson, 2002]:

$$S(\omega) \propto \omega^{-2H-2} \tag{6}$$

H =1/3 for all the simulations.

H is also related to the fractal dimension of contour lines that enclose areas which have a (log) rain rate greater than a given threshold [Voss, 1985]. H controls the fractal dimension of the resulting simulated rain field.

The surfaces are generated on a lattice in an iterative manner. On a square grid, the generation of a midpoint displacement surface has two stages for each step. Figure 18 gives a conceptual flowchart of the whole simulation process, while figure 19 gives a schematic representation of the iterative additive procedure described below.

The first step is the generation an independent Gaussian variable ξ with zero mean and unit variance. This value is used as the level at the central point on the lattice (point A). The four corner points (points B) of the lattice are given a value equal to zero. The values at the midpoints (points C) of each of the four lines on the outside of the lattice are the average of the two end points and the centre point, i.e. the value at the midpoint of the line is given by the average of the values of its nearest neighbours. Then, points inside the lattice (points D) are given values according to the average of their diagonal neighbours. All the points plotted then have independent values of $\xi_{n=1}$ added to them, where the Gaussian random variable now has the variance given by:

$$\left\langle \xi_n^2 \right\rangle = \sigma_n^2 = r_l^{2nH} \tag{7}$$

with

$$r_l = 1/\sqrt{2} \tag{8}$$

and

$$n=1. \tag{9}$$

This determines a new square lattice at 45° to the original with lattice size $1/\sqrt{2}$.

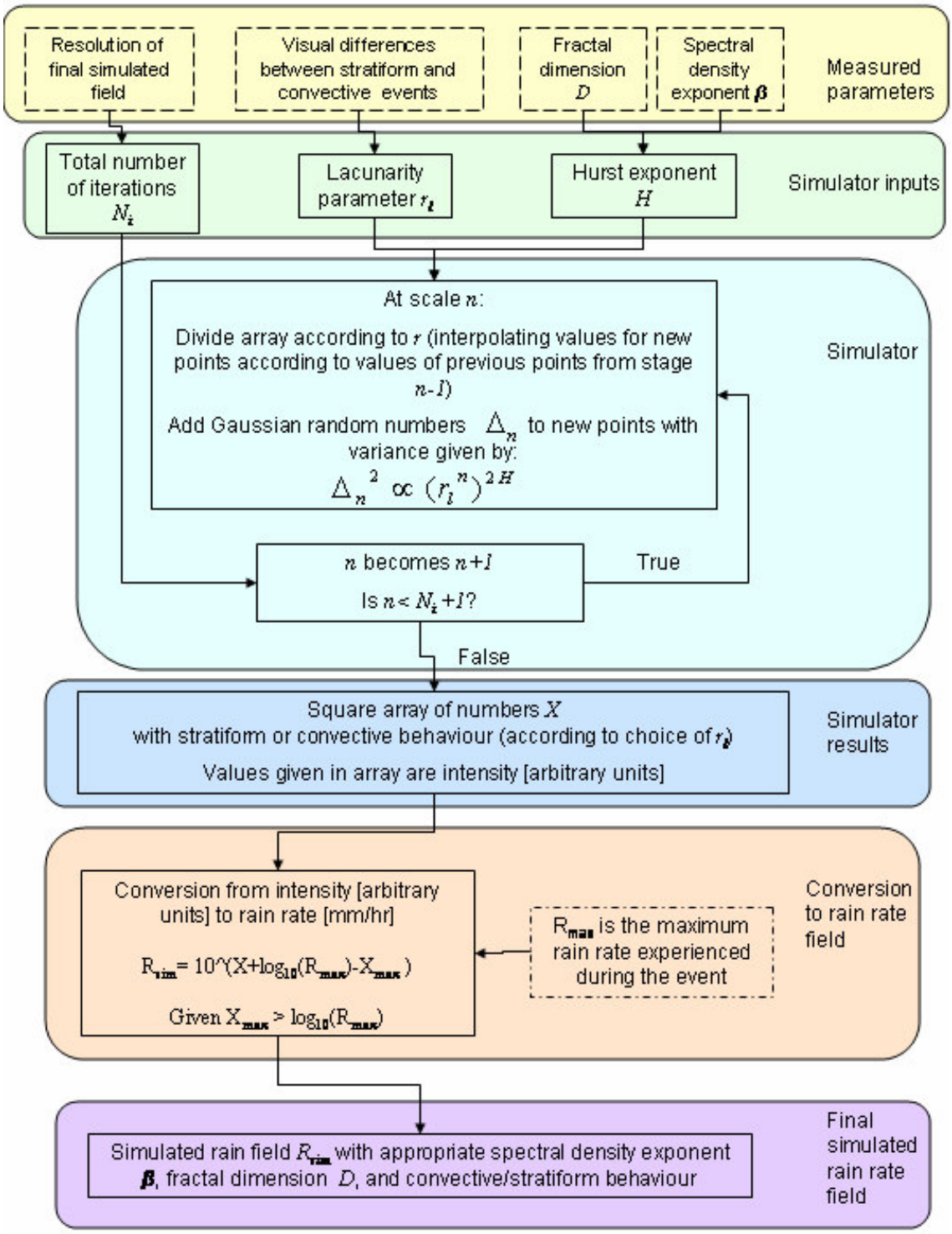

Figure 18: conceptual flowchart of the simulation process.

The procedure is continued for the next generation (points E) where the values at the new points are given by the average of the nearest neighbour locations, i.e., the neighbours in directions parallel to the axes. The points on the rim will have values given by the average of their three nearest neighbours, rather than sites inside the lattice, which have four. All the points plotted

then have independent values of $\xi_{n=2}$ added to them, with the variance given by the equation above. This produces the new square lattice with a scale 1/2 the original.

Each generation has the variance changed according to stage *n* and the process continues until all the points on the lattice are filled. The result of the algorithm is a two-dimensional array of values, X, with a side length of $2^{N_i}+1$, where N_i is the total number of iterations. N_i is effectively only limited by the speed and memory capabilities of the computer used for the simulation. On a desktop PC with 512 MB of RAM and a processor speed of 2.4 GHz, the time taken to create a simulated rain field with N_i=10 and $r_l = 1/2$ is less than 5 seconds. As a batch, generating 50 2D simulated stratiform events takes ~8 minutes (with each simulated stratiform array 1025*1025 pixels square) and generating 50 2D simulated convective events takes ~6 minutes (with each simulated convective array 730*730 pixels square).

Differentiating between simulations of stratiform events and convective events requires the changing the value of the parameter r_l. This parameter controls whether or not all the rain occurs in one large area (as is the case for stratiform rain) or instead is broken up into convective type rain cells. It is related to the concept of "lacunarity" discussed in [Mandelbrot, 1983, Feder, 1988].

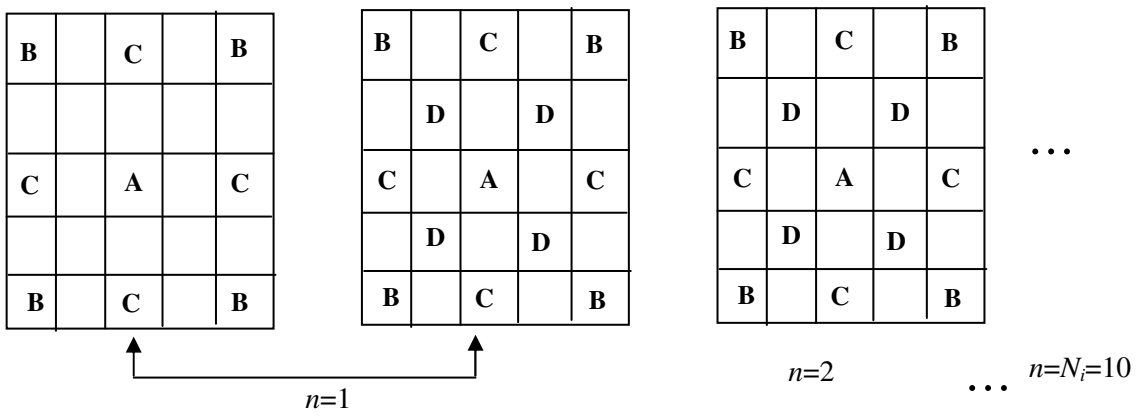

Figure 19: Schematic diagram of the successive random addition method for simulating fractional Brownian motion in 2 dimensions. For simplicity, the stage n=1 is broken up into two steps in the diagram.

A fractal is called lacunar if it contains large intervals or gaps in the fractal set (or measure). In the case of our data and simulations, stratiform rain fields are more lacunar, i.e., the gaps between areas of stratiform rain tend to be larger than the gaps between the convective rain cells, which are more fragmented, but closer together. In some cases the gaps between areas of stratiform rain are so large that we only see one area of rain at a time in the radar scans. In the case of strictly self-similar fractals (such as the Cantor set) varying the lacunarity does not alter the fractal dimension. However, for statistically self-similar fractals, such as the random fractal fields presented here, changing the lacunarity can impact the spectral density function, and hence the fractal dimension (see section 2.3.5 for more details).

The successive random addition algorithm described above uses the same algorithmic procedure as for the midpoint displacement algorithm [Voss, 1985], in which r_l is fixed with a value of 1/2 (though for each step in the simulation there are two stages, with r_l being reduced by $1/\sqrt{2}$ at each stage). However, because with successive random additions all points are treated

equivalently at each stage, the resolution at the next stage can change by any factor [4] $r_l < 1$. For the simulations presented here, empirically chosen values of $r_l = 1/2$ and $r_l = 1/3$ are used for stratiform and convective rain respectively. This is because the concept of lacunarity does not yet have the required mathematical development, in contrast with the concept of fractal dimension, and therefore there is very little in the literature about how to calculate it for real data. This is clearly an area of future research.

Given a sample of N_n points at stage n with resolution λ, stage $n+1$ with resolution $r_l\lambda$ is determined first by interpolating the values at the new resolution, from the old N_n values, where the number of points plotted at the new resolution is:

$$N_{n+1} = (\frac{1}{r_l^{n+1}} + 1)^2 \tag{10}$$

A random element Δ_n is then added to all N_{n+1} points, where at stage n, with scaling ratio $r_l < 1$. Δ_n is a Gaussian random variable, with zero mean and a variance given by:

$$\Delta_n^2 \propto (r_l^{\,n})^{2H} \tag{11}$$

The successive random addition algorithm can also be implemented in three dimensions.

The resulting arrays are equivalent to log rain rate fields, hence some processing is required to convert to equivalent rain rates. Figure 20 plots the cumulative distribution functions of the three different measured rain events in comparison with 2D and 3D simulated rain fields. As can be seen, the shape of the simulated curves are similar to the measured curves, with the exception that the measured curves are truncated at a log rain rate value of -1.5. The simulated curves have a higher mean than the measured ones, and so have to be offset in order to make them equivalent to $\log_{10}$(rain rate) (mm/hr).

This can be done by using the following formula:

$$R_{sim} = 10\text{^}(V + \log_{10}(R_{\max}) - V_{\max}) \tag{12}$$

where V is the simulated array values, V_{max} is the maximum value in V, R_{max} is the maximum rain rate experienced during the event and R_{sim} is the resulting simulated array of rain rates. (V_{max} must be greater than $\log_{10}(R_{max})$)

This offset will alter the mean of the simulated distribution but will not affect any of the higher order moments. On a strict mathematical basis, using the maximum value of a distribution to alter the mean of the distribution is not recommended. However, for our purposes, and solely on an event by event basis, the maximum rain rate is a convenient metric. Further work should be done in this area in order to make the conversion to equivalent rain rates more mathematically rigorous, and is planned for the extension to this project.

[4] In the literature of discrete cascades mentioned earlier, r_l can be assumed to be related to the branching number of the cascade.

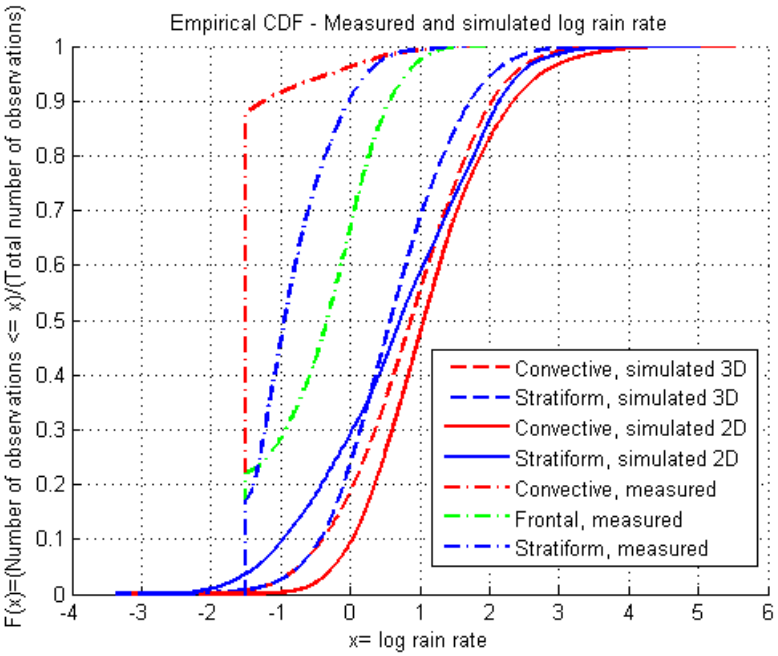

Figure 20: Cumulative distribution functions of log rain rate events and simulated arrays (2D and 3 D)

Figure 21 shows the results of this final conversion, and plots the measured and simulated rain fields. On an event by event basis, the simulated events compare reasonably well with the measured events. The variation between the simulated and measured fields is potentially due to inter-event variability. Again, further work on the rain field simulator using a statistically significant database of measured and simulated rain fields would be advised.

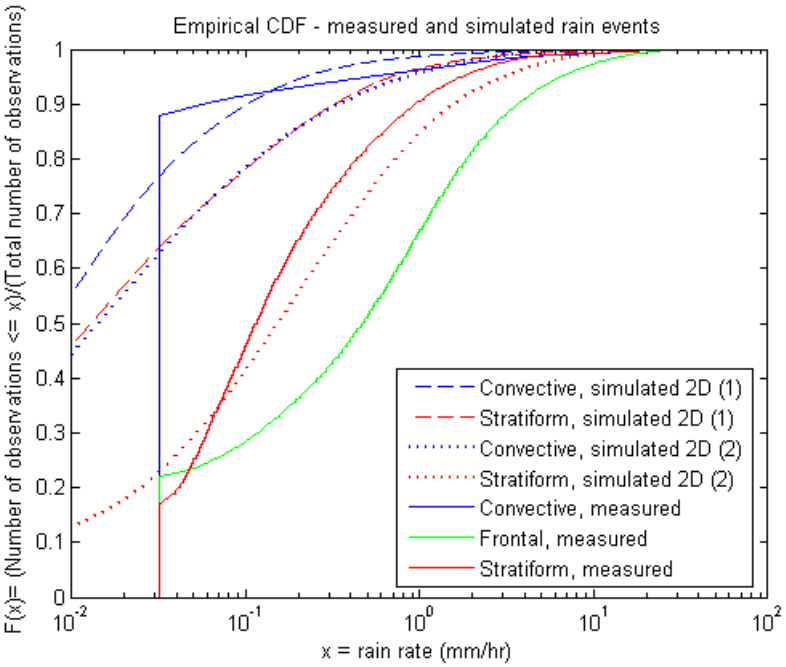

Figure 21: Cumulative distribution functions of rain rate events and equivalent simulated 2D rain fields

The resulting simulated rain field has appropriate spectral density exponent, fractal dimension, and behaviour that is visually consistent with experimentally observed convective or stratiform type events (according to what is desired). Figures 22a and 22b show examples of simulated stratiform and convective rain fields.

2.3.4 Temporal variation in the simulator

The time variation of the two-dimensional simulated rain field was achieved through the use of Taylor's frozen storm hypothesis [Taylor, 1938]. This hypothesis postulates the equivalence between the spatial autocorrelation at a fixed point in time and the temporal autocorrelation at a fixed position in space. However, for this to hold, the spatial argument of the former must be interpreted as a time lag of the latter and the spatio-temporal field must be a fixed spatial field moving with a constant velocity. It has been shown [Zawadski, 1973] that this holds approximately for time lags under about 40 minutes, which is a timescale much longer than what is needed to implement ATPC.

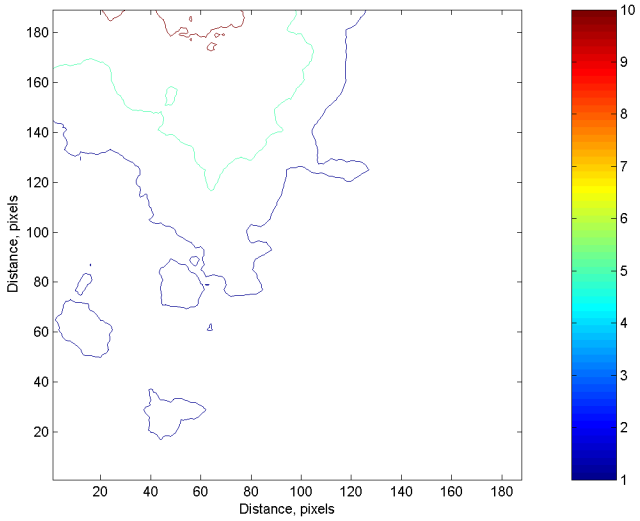

Figure 22a: Example of simulated stratiform rain field.

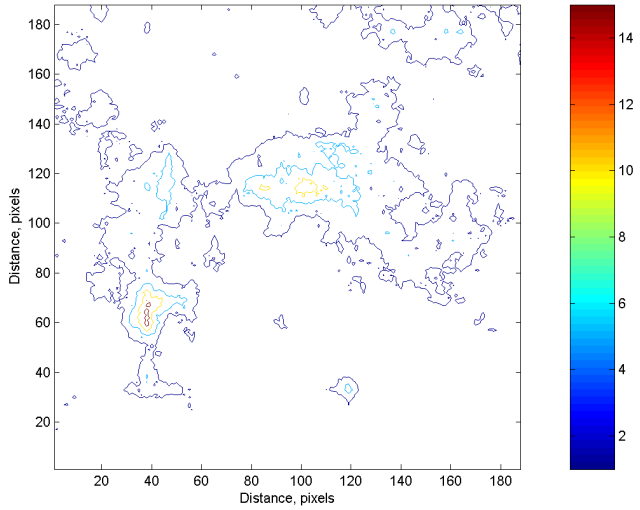

Figure 22b: Example of simulated convective rain field.

To implement this time variation, each simulated rain field was cut down into a number of smaller "snapshots" of 200*200 pixels. Within these snapshots, the location of the simulated

links are fixed. The variation in time was simulated by moving the position of the snapshots in the full-size simulated array by a small amount Δx and Δy, then saving the resulting new snapshot to give the rain field at time $t=1$. The process was repeated to give snapshots at time $t=t...n$. Δx and Δy were chosen to give similar wind velocities as those experienced during the measured rain events.

The time resolution of the simulated data can be varied by making each simulated pixel cover a smaller area. However, this would then reduce the number of snapshots that could be extracted from the full-size array, leading to fewer measurements in time.

The successive random addition algorithm can also be implemented in three dimensions to give a temporal variation provided by the third dimension of the array. This assumes an equivalency of time and space, and provides simulated rain fields which evolve in time, but do not advect. Unfortunately, due to the finite amounts of memory available in the PC generating the rain fields, the increasing the number of dimensions in the simulated array comes at the cost of decreasing the total area covered by the array. For example, a simulated two-dimensional stratiform rain field has N_i =10, and a side length of 1025 pixels. A simulated three-dimensional stratiform array has N_i =7, and a side length of 129 pixels.

Each run of the simulator produces a single realisation of a rain field, either in two or three dimensions. Due to the random nature of the generation process, there will not be temporal correlation between two different simulated rain fields, however space correlation occurs within each single realisation.

The simulator is capable of producing stratiform-like and convective-like synthetic rain fields, with fractal dimension of contour lines enclosing areas of rain greater than or equal to a threshold, and a spectral density function exponent and spatial autocorrelation function consistent with measured data.

Further work on the simulator is planned in order to tie the conversion from simulated arrays to equivalent rain rates more rigorously to statistical rain rate parameters, and to convert the simulator from an event-on-demand generator, to a procedure capable of simulating longer time series (daily, monthly, annual) of rain rate data.

2.3.5 Application of simulated rain fields to the analysis software

Ideally, for the rain fields to use with the analysis software, we would like a 'test' area of 25 km x 25 km, with a 10 km margin either side i.e. 45 km x 45 km total. The resolution of the rain field should be 1 pixel equivalent to an area 100m x 100m. These requirements for the simulated rain fields are based on the observation that almost all interfering paths are less than 5 km and a 25 km square in London has ~ 1000 links.

Figures 23 (a and b) show the radial sections through the two-dimensional spatial autocorrelation function for the simulated fields. If we compare these to figures 7a and 7c we see that the correlation factor of the simulated fields falls off more quickly with distance than the measured fields(on a pixel by pixel comparison). If each simulated pixel is considered to be equivalent to an area of 100m*100m, then the correlation of the simulated rain field doesn't agree completely with the measured statistics. The worst case for ATPC occurs when the rain fields are completely de-correlated, so using the simulated fields means that the simulations are more realistic than the worst (totally de-correlated case) but are not as realistic as the measured data.

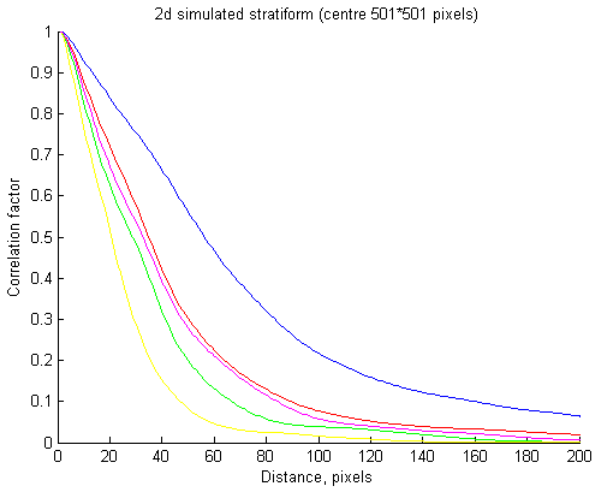

Figure 23a: Radial sections through the spatial autocorrelation for a 2D simulated stratiform event

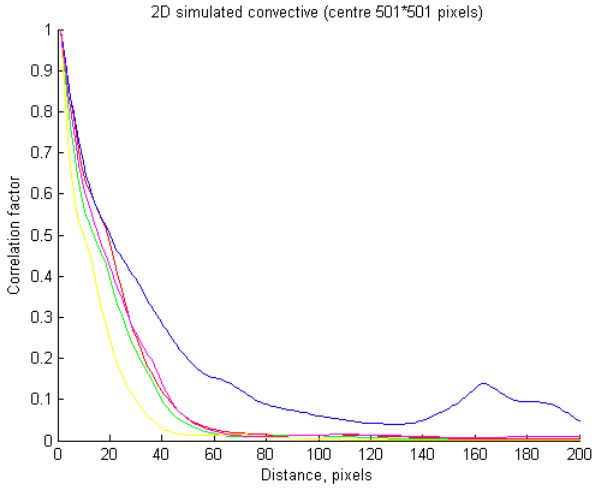

Figure 23b: Radial sections through the spatial autocorrelation for a 2D simulated convective event

It is possible to modify the rain field simulator to produce simulated rain fields where that the correlation factor falls off more slowly with distance. This is done by altering the lacunarity i.e. for r_l>1/2. Figure 24 shows an example field where r_l is 5/6 and figure 25 shows the corresponding radial sections through the spatial autocorrelation function.

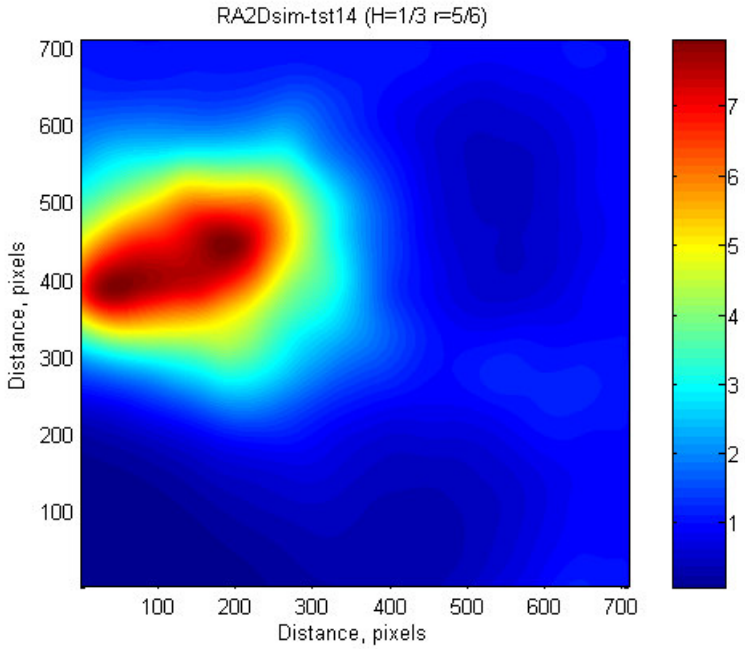

Figure 24: Example simulated rain field where r_l = 5/6

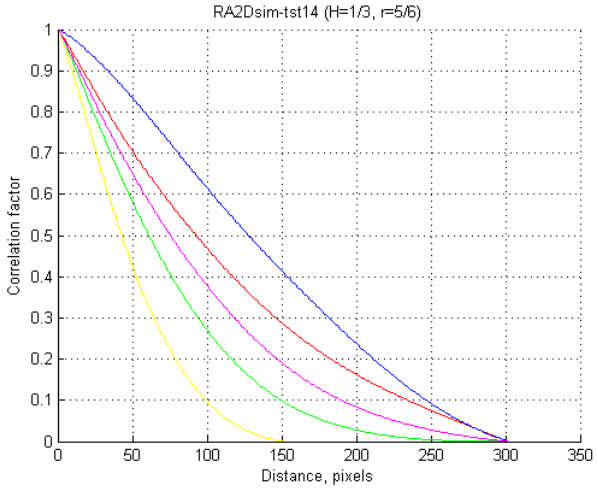

Figure 25: Radial sections through the spatial autocorrelation for a 2D simulated event where r_l = 5/6

As can be seen, this change in the lacunarity smoothes out the variation in the simulated rain field – changing the fractal dimension of the contour lines and the spectral density exponent.

Stochastic modelling using Gaussian statistics (as used here) and the second order moments may be termed spectral modelling, since the noise autocorrelation function and the power spectrum specify equivalent information and are in fact a Fourier transform pair [Lewis, 1987]. Appendix 1 gives more information on this relationship. Hence using the lacunarity to alter the autocorrelation function affects the power spectral density function, which in turn impacts on the fractal dimension of the simulated field.

As stated before, the lacunarity has not yet had the thorough mathematical grounding that the concept of fractal has, hence the uncertainty in its application is not surprising.

In order to investigate whether the behaviour of the fall-off of the radial spatial autocorrelation with distance is affected by the number of pixels or pixel size of the array, the following figures were plotted. Figure 26a shows the radial spatial correlation factor fall-off with distance for the measured convective event with the data for the autocorrelation calculation limited to the centre 95*95 pixels in the 188*188 pixel original array. Figure 26b shows the same but with the data for the autocorrelation calculation effectively being the entire measured array, but degraded to a lower resolution where 1pixel=600m*600m. This degradation was achieved by setting each new pixel in the degraded array to the average of the four pixels in the non-degraded array that the new pixel covered.

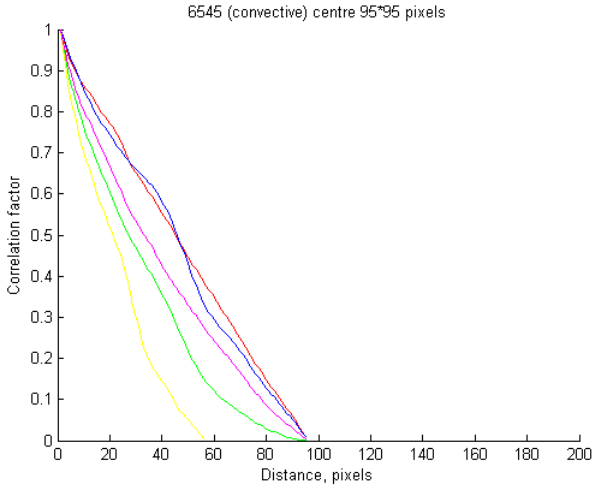

Figure 26a:Radial spatial correlation factor fall-off with distance – measured convective event (centre 95*95 pixels)

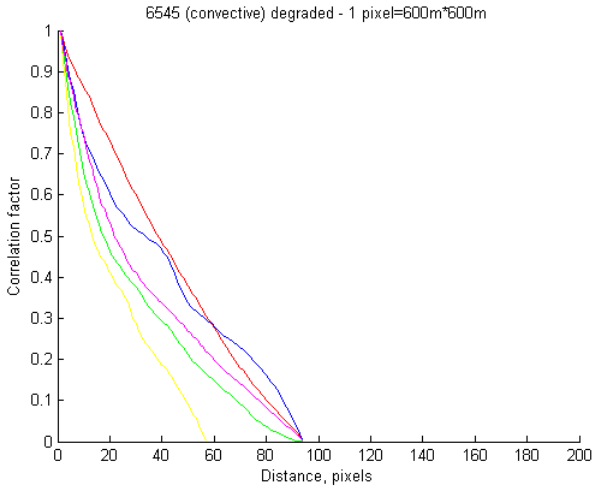

Figure 26b:Radial spatial correlation factor fall-off with distance – degraded convective event (1pixel=600m*600m)

As can be seen from these figures, it appears that the correlation factor falls to zero at the edge of the sampled array, no matter the array size i.e. the tail of the distribution is affected by the number of pixels in the array. The head of the distribution, which is the part we're most interested in seems unchanged. This indicates that the resolution of the data used does impact the fall-off of the autocorrelation function, but predominantly affects the tail of the curve.

A further literature search was carried out to determine what rain field data at small scales (i.e. on a pixel size of 100m *100m) was available. Gebremicheal et al [2004] present results from two TRMM campaigns, looking at the ability of radar-derived rainfall products to characterise the small scale spatial variability of rainfall. Figure 2 in the paper (reproduced below as figure 27) suggests that the correlation measured from these datasets falls off with distance at a comparable rate to the simulated stratiform rain fields shown earlier (assuming that 1 pixel = 100m *100m).

This is confirmed by another paper [Moszkowicz, 2000] where the small scale spatial autocorrelation of rain fields was determined for distances from 10 m to several 10s of km using a rain gauge network for distances from 10m to 5 km and a radar for distances from 2 to 10 km.

These papers suggest that the model used here is physically realistic in terms of small scale spatial autocorrelation. However, there is limited rain field data available at these resolutions, hence further study is advised.

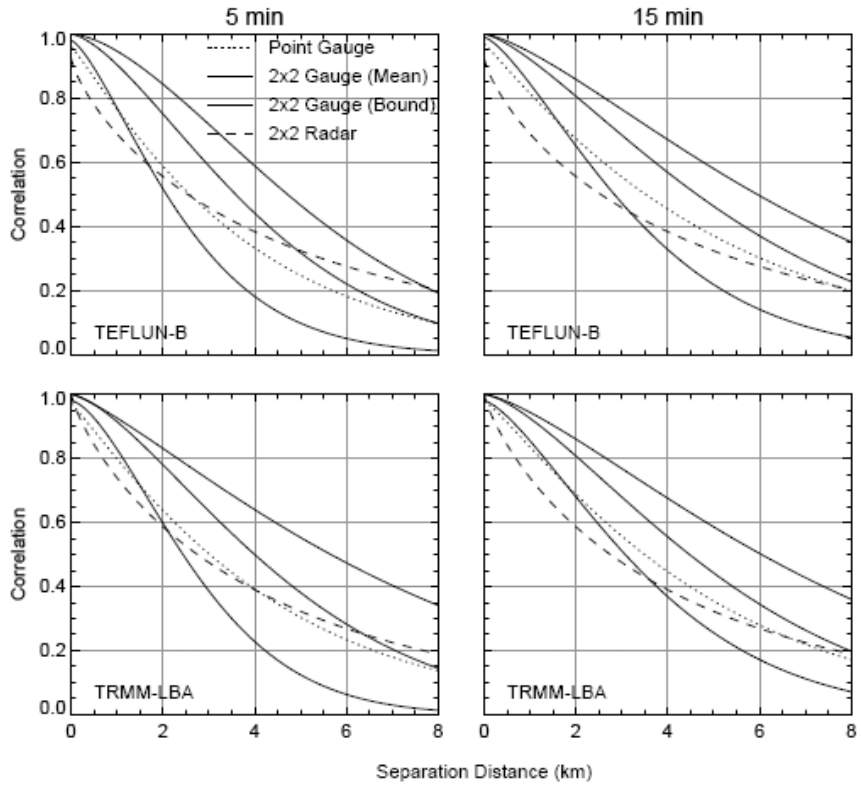

Figure 27. Spatial point- and area-correlation function estimated from gauge-rainfall fields, and the uncertainty bound for the area-correlation function. Also shown is the correlation function estimated from radar-rainfall fields. [Gebremichael et al, 2004]

3. ATPC system definition

The basic principle for ATPC is quite simple. In cases where rain fading occurs on the radio path, it involves increasing the transmit power to compensate for the fade. Given a reliable power control system, it is possible to reduce the fixed fade margin during clear sky conditions (i.e. no fading), thereby improving the rate of frequency reuse and link packing density in the geographical area of the link. This is because lower fade margins use less transmit power, which lessens the interference on adjacent links.

3.1 ATPC parameters

The operating capability of the transmit terminal is defined by the EIRP levels P_{min} and P_{max} where:

- P_{max} is effectively determined by the maximum EIRP specified by the regulator in order to satisfy a given availability requirement
- P_{min} is determined by the performance of the equipment

$P_{max} – P_{min}$ is the ATPC range.

3.2 Setting up the link

The nominal operating condition (i.e. the condition that the ATPC seeks to preserve) is set at a receive signal level a number of dB greater (e.g. 3 to 7 dB) than the 10^{-6} BER sensitivity level, referred to by Ofcom as the Receiver Sensitivity Level (RSL). The 3 to 7 dB margin above the RSL is either called the offset or the remote fade margin. The nominal operating condition is set to provide a BER of the order of 10^{-11} or 10^{-12} in order to ensure that the Background Block Error Rate (BBER) is no more than would be the case were ATPC not to be used [ETSI TR 101 036-1 v1.3.1 2002-8].

In setting up the link it is necessary to specify P_{max}, in accordance with the maximum EIRP permitted, and to specify the receive signal level associated with the nominal operating condition. When initially setting up the link under nominal propagation conditions the ATPC immediately adjusts the power by way of a transmitter / receiver closed loop to establish the nominal operating condition.

Figure 28 graphically represents the issues raised in the following sections.

3.2.1 ATPC range exactly matched (Black line)

In the ideal case the total fade margin associated with the required availability for the link = the ATPC range + the remote fade margin.

The nominal operating power of the transmitter as established by the ATPC loop would be exactly P_{min}.

$$EIRP_{nominal} = EIRP_{max} – \text{Total fade margin} + \text{Remote fade margin}$$

or

$$EIRP_{nominal} = EIRP_{max} – \text{ATPC range}$$

3.2.2 ATPC range greater than the matched situation (Green line)

In the case where the ATPC range is greater than that in the matched case above, P_{min} of the equipment is less than the transmitter power required to establish the nominal operating condition. On set-up the ATPC loop automatically adjusts the transmitter power to a level higher than the equipment's P_{min} and sufficient to establish the nominal operating condition.
The nominal operating power of the transmitter ends up at a level the same as the matched situation above but higher than the equipment's P_{min}

In enhanced propagation conditions it can be expected that the ATPC loop will reduce the transmitter power as appropriate, but only down to P_{min} of the equipment as the limit, in order to maintain the nominal operating condition.

$$EIRP_{nominal} = EIRP_{max} - \text{Total fade margin} + \text{Remote fade margin}$$

3.2.3 ATPC range less than the matched situation (Red line)

In the case where the ATPC range is less than that in the matched case above, P_{min} of the equipment is higher than the transmitter power required to establish the nominal operating condition. On set-up the ATPC loop can therefore only adjust the transmitter power down to P_{min}.

As a fade occurs the ATPC loop will not start to operate (i.e. increase the transmitter power) until the received signal level has fallen (due to the fade) to the specified nominal operating condition.

The nominal operating power of the transmitter is at P_{min} of the equipment which is higher than the matched situation above and which under nominal propagation conditions will provide a received signal level higher than absolutely necessary.

$$EIRP_{nominal} = EIRP_{max} - \text{ATPC range}$$

3.2.4 Summary—for planning purposes

When ATPC range $\geq$ Total fade margin – Remote fade margin

$$EIRP_{nominal} = EIRP_{max} - \text{Total fade margin} + \text{Remote fade margin}$$

When ATPC range < Total fade margin – Remote fade margin

$$EIRP_{nominal} = EIRP_{max} - \text{ATPC range}$$

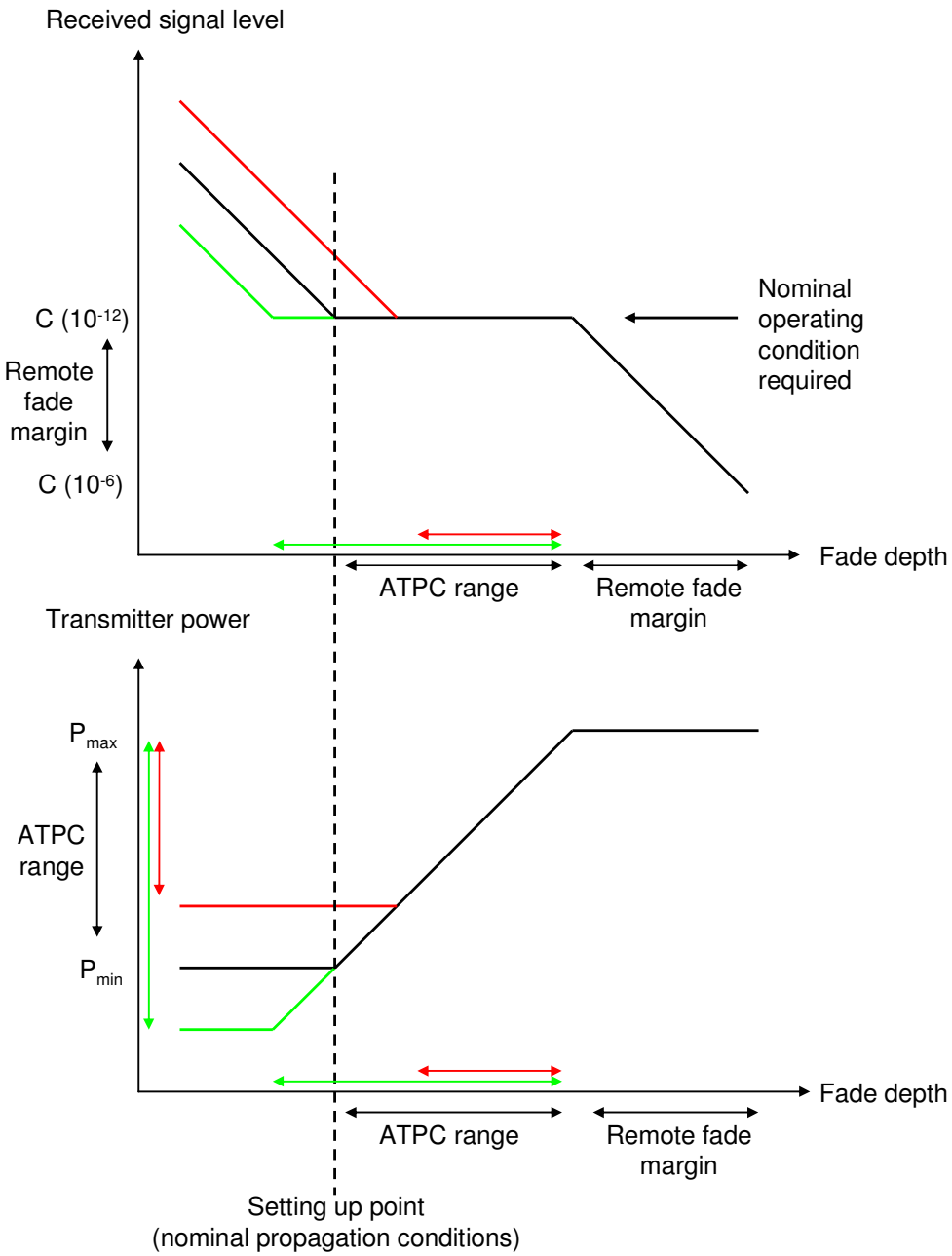

Figure 28: Graphical representation of ATPC range matching

4. ATPC implementation tool

As described in [Richardson et al, 2004], there are four general cases to consider:

Case 1—Mixed ATPC and non-ATPC deployment, with uncorrelated fading.
Case 2—Mixed ATPC and non-ATPC deployment, with correlated fading.
Case 3—All-ATPC systems, with uncorrelated fading.
Case 4—All-ATPC systems, with correlated fading.

Whether or not the fading is correlated depends on the type of fading and the distance between the wanted and interfering links. As we have seen earlier, rain field correlation falls off quickly with distance, hence links that are greater than ~50 km apart can be considered to be very weakly or un-correlated.

For a system operating at frequencies below about 10 GHz the main fading mechanism is multi-path interference. In this situation the fading on the wanted and the unwanted links are, for all practical purposes, uncorrelated and Cases 1 and 3 apply.

For systems operating above about 15 GHz, multi-path is not the dominant fading mechanism due to the short path lengths and instead fading due to rain attenuation becomes the dominating factor. Cases 2 and 4 apply for radio links of short length and which are a small distance apart. Hence, situations where it is possible to claim a co-ordination advantage and achieve a gain in spectrum utilisation and packing density are dependent on the link layout and the geographical area covered.

These cases have been investigated by the use of a simulator developed for the purpose of this study. The simulator has two parts: a planning tool, which plans a set of links using standard planning assumptions, and an analysis tool, which takes a plan produced by the first tool and examines the response of the links to a sequence of rain fields.

4.1 Planning tool

The planning tool takes an existing plan and re-plans it, subject to a number of assumptions:

- the mix of ATPC and non-ATPC links
- the type of ATPC in use.

The statistics of the new plan are then calculated to estimate changes in band efficiency.

The initial plan was based on the existing 38 GHz band plan supplied by Ofcom. The 13,949 links in the initial plan were filtered to remove links for which the data appeared to be incorrect (76 links), for which antenna patterns could not be found (165 links) or which failed the Fresnel zone test (52 links)—leaving 13,656 links, located throughout the UK; one link is one-way, the remainder are two-way; all links are vertically polarised.

The planning process follows OfW 42, with some exceptions:

- the links are not checked against the ‘minimum path length policy’
- there is no 6 dB EIRP uplift for obstructed paths
- antenna pointing is calculated by the application—the plan value is discarded.

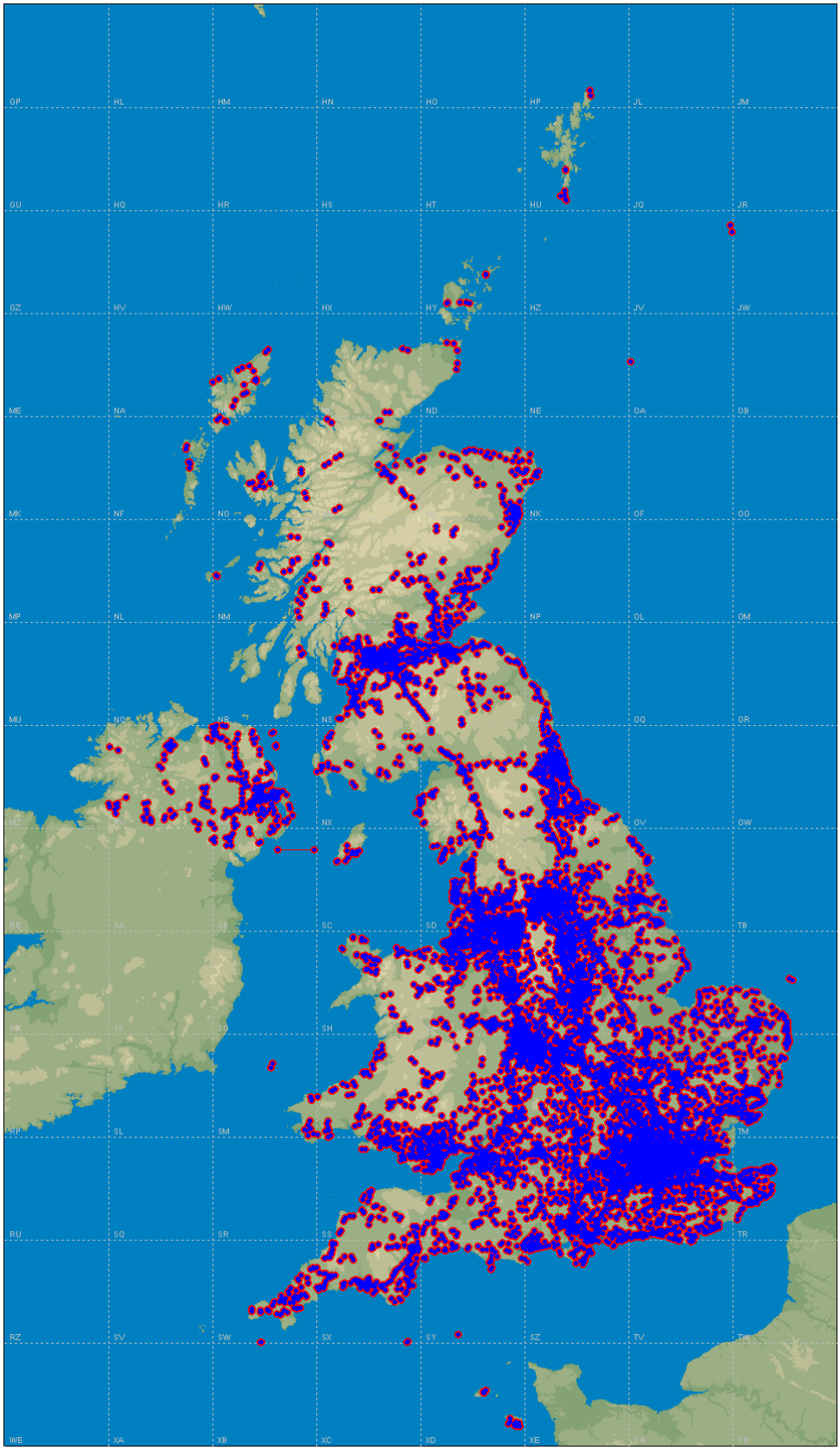

Figure 29: Link distribution in the UK in the 38 GHz band

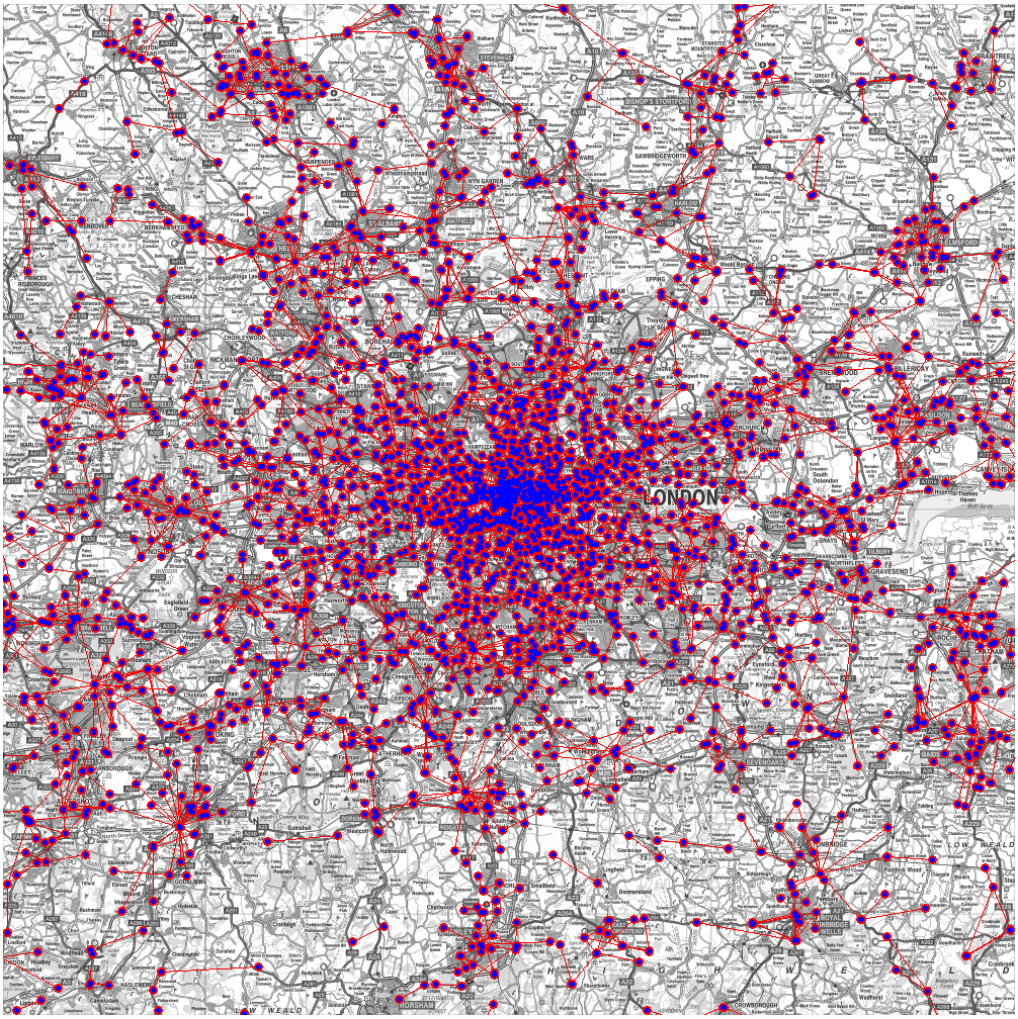

Figure 30: Link distribution in London in the 38 GHz band

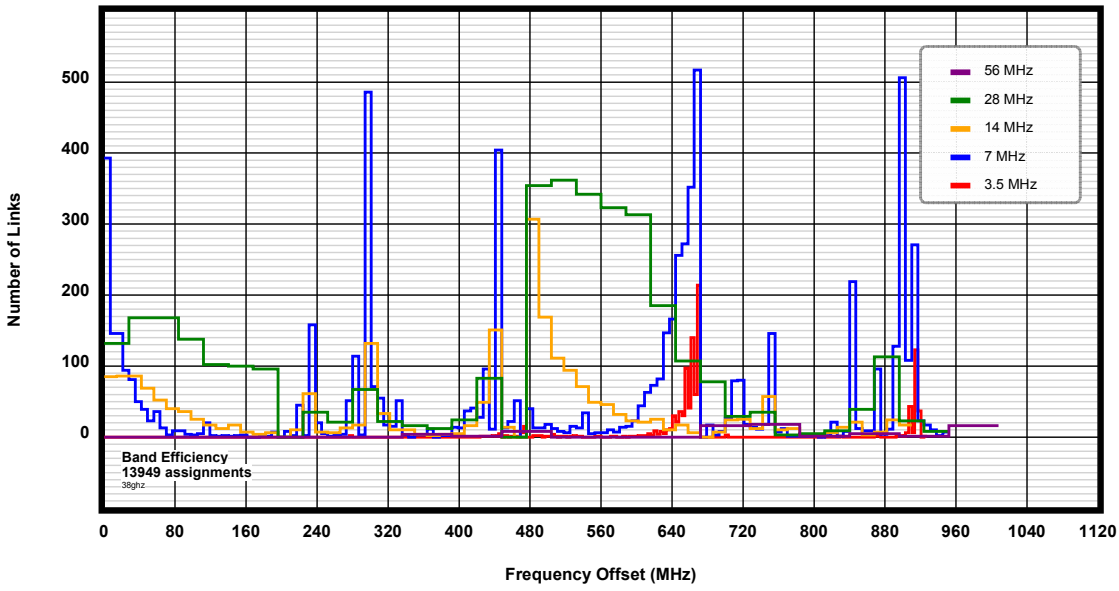

Figure 31: Existing assignments in the 38 GHz band

Plans have been run using the two ATPC methods described earlier:

- assigned EIRP is offset by a constant positive amount[5] from $EIRP_{non\text{-}ATPC} - FM$.
- assigned EIRP is offset by a variable negative amount[6] from $EIRP_{non\text{-}ATPC}$.

Plans have also been run for two orderings of the link data—forward and reverse—which tests the stability of the results against assumptions about link geometry.

In practice, the automatic planning software was unable to assign every link because of high-low clashes. The number of such clashes was, however, greatly reduced by grouping links that share masts into pseudo-networks before frequencies were assigned[7].

4.1.1 Re-planning the 38 GHz band

The effect of re-planning the band with the automated planning application results in a contraction of the assignments to the lower end of the band (see figure 32).

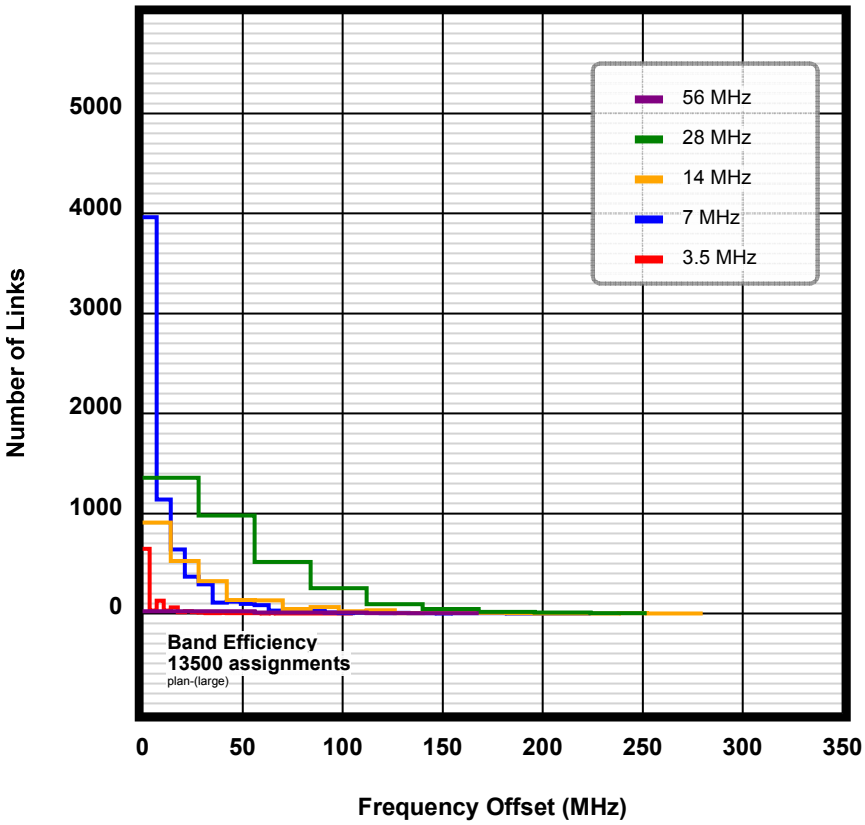

Figure 32: Automated re-plan (no ATPC)

[5] The offset is variously called 'remote fade margin' or 'operating margin'. This method assumes the ATPC equipment is capable of covering the difference between the remote fade margin and the fade margin.

[6] The offset is normally the ATPC range: however, the reduced EIRP is constrained to provide the required remote fade margin.

[7] For example, the total number of assigned links increased from 12,781 to 13,500 for the non-ATPC plan, and from 12,805 to 13,527 links for an all-ATPC plan with a remote fade margin of 5 dB. The supplied database does not contain any information about actual networks.

The effect of introducing 'ideal' ATPC on all links is apparent when comparing figures 33 and 34 (RFM is 5 dB): both the number of assignments in the first channel and the maximum bandwidth are significantly improved. The number of links assigned to the first channel rises from 51% to 75%; the maximum bandwidth decreases from 280 MHz to 168 MHz.

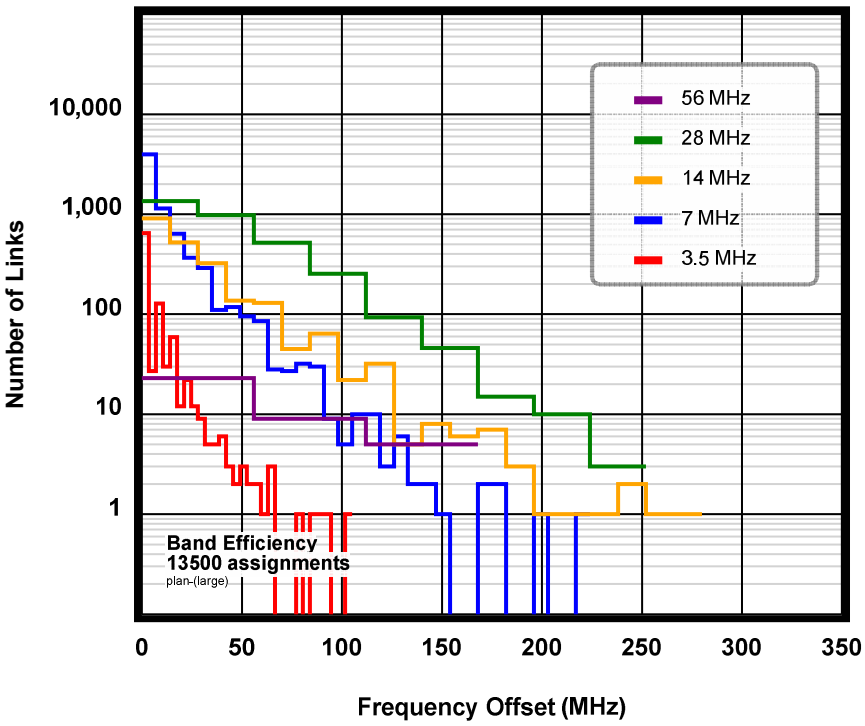

Figure 33: Automated re-plan (no ATPC)—log scale

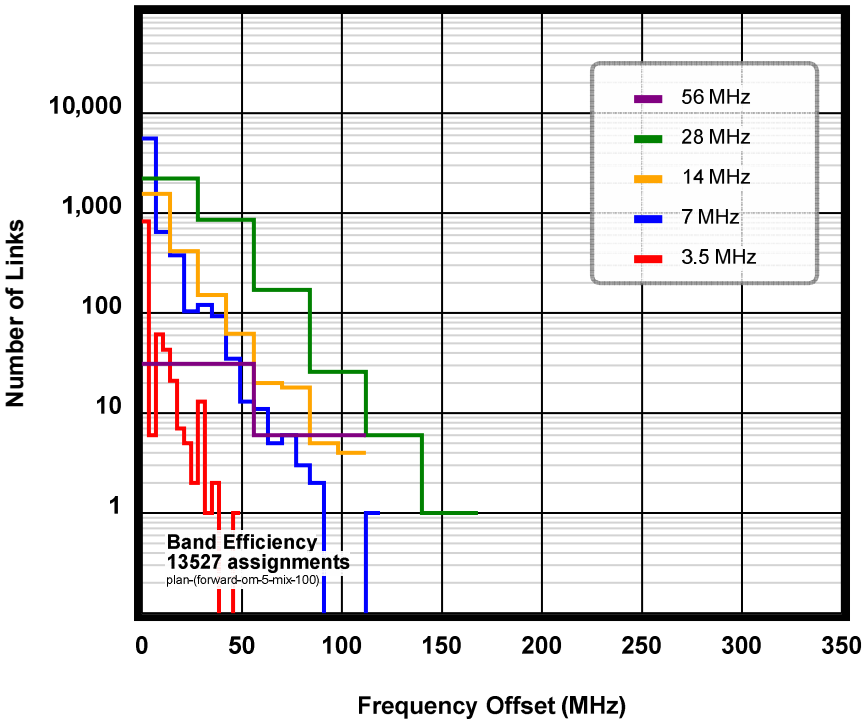

Figure 34: Automated re-plan (all ATPC, RFM = 5 dB)—log scale

A more realistic method of modelling ATPC was also considered, in which the non-ATPC EIRP was backed-off by a constant offset (i.e. the ATPC range), subject to satisfying the RFM. The following plan (figure 35) was produced for an assumed ATPC range of 10 dB and an RFM of 5 dB: the result of imposing the constraining effect of a limited ATPC range is to reduce the plan efficiency as compared with the 'ideal' case (figure 34).

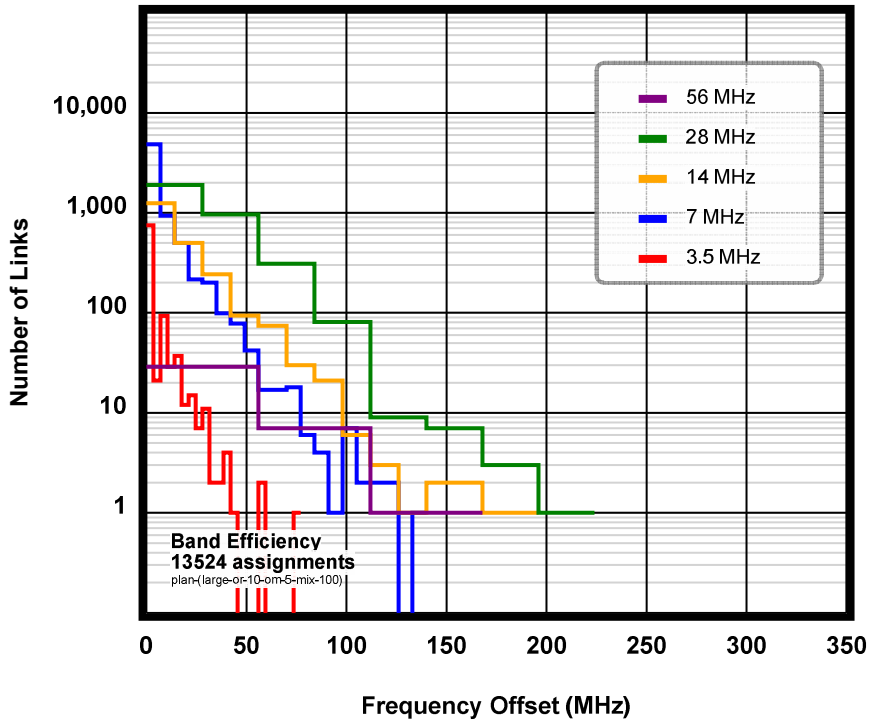

Figure 35: Automated re-plan (all ATPC, range = 10 dB, RFM = 5 dB)—log scale

The statistics of these plans are shown in the following tables.

Channel Spacing (MHz)	Maximum Channel Number	Number of Channels Used	BW (MHz)	Total Number of Assignments	Number of Assignments in Channel 1
3.5	30	24	105	985	648
7	32	26	224	6981	3962
14	20	20	280	2225	909
28	9	9	252	3272	1357
56	3	3	168	37	23
			280	13500	6899

Table 3: Plan statistics (non-ATPC)

Channel Spacing (MHz)	Maximum Channel Number	Number of Channels Used	BW (MHz)	Total Number of Assignments	Number of Assignments in Channel 1
3.5	14	12	49	988	825
7	17	14	119	6992	5571
14	8	8	112	2232	1556
28	6	6	168	3278	2217
56	2	2	112	37	31
			168	13527	10200

Table 4: Plan statistics (all ATPC, RFM = 5 dB)

Channel Spacing (MHz)	Maximum Channel Number	Number of Channels Used	BW (MHz)	Total Number of Assignments	Number of Assignments in Channel 1
3.5	22	15	77	988	750
7	20	19	140	6992	4841
14	14	14	196	2229	1250
28	8	8	224	3278	1900
56	3	3	168	37	29
			224	13524	8770

Table 5: Plan statistics (all ATPC, ATPC range = 10 dB, RFM = 5 dB)

4.1.2 Variation of plan efficiency

To explore the stability of the efficiency measurements a number of sensitivity analyses have been performed:

- variation of remote fade margin (RFM)
- variation of ATPC range
- variation of ATPC/non-ATPC mix.

The results are shown in the figures 36 and 37[8].

The following general characteristics are apparent:

- the higher the ATPC penetration, the higher the efficiency
- the more capable the ATPC equipment, the higher the efficiency
- realistic RFM values (e.g. 3–7 dB) are generally the most efficient

The implementation of ATPC in the 38 GHz band gives significant improvements in spectrum efficiency as measured by the increase in the number of links assigned to channel 1 (from ~50% to ~70%) or the decrease in the maximum bandwidth used (from ~300 MHz to ~180 MHz).

[8] The results are the average of plans based on 'forward' and 'reverse' ordering of the base 38 GHz plan.

ATPC Range (dB)[9]

ATPC: 0%		*0*	*5*	*10*	*15*	*20*	*25*	*FM–RFM*
	0	51.4%	51.4%	51.4%	51.4%	51.4%	51.4%	51.4%
	2	51.4%	51.4%	51.4%	51.4%	51.4%	51.4%	51.4%
RFM (dB)	*4*	51.4%	51.4%	51.4%	51.4%	51.4%	51.4%	51.4%
	6	51.4%	51.4%	51.4%	51.4%	51.4%	51.4%	51.4%
	8	51.4%	51.4%	51.4%	51.4%	51.4%	51.4%	51.4%
	10	51.4%	51.4%	51.4%	51.4%	51.4%	51.4%	51.4%

ATPC: 25%		*0*	*5*	*10*	*15*	*20*	*25*	*FM–RFM*
	0	51.4%	52.8%	53.7%	53.8%	53.8%	53.6%	53.2%
	2	51.4%	52.9%	53.9%	54.4%	54.5%	54.5%	54.4%
RFM (dB)	*4*	51.4%	52.9%	54.1%	54.7%	54.9%	55.1%	55.0%
	6	51.5%	53.0%	54.2%	54.7%	55.1%	55.2%	55.2%
	8	51.5%	53.0%	54.2%	54.7%	55.0%	55.1%	55.2%
	10	51.4%	53.0%	54.0%	54.6%	54.8%	54.9%	54.9%

ATPC: 50%		*0*	*5*	*10*	*15*	*20*	*25*	*FM–RFM*
	0	51.4%	54.6%	56.4%	57.6%	58.1%	58.1%	57.9%
	2	51.4%	54.6%	56.9%	58.5%	59.2%	59.4%	59.4%
RFM (dB)	*4*	51.5%	54.7%	57.2%	58.9%	59.7%	60.0%	60.1%
	6	51.5%	54.9%	57.3%	59.0%	59.8%	60.1%	60.3%
	8	51.5%	54.8%	57.3%	58.8%	59.6%	59.9%	60.0%
	10	51.4%	54.7%	57.0%	58.4%	59.0%	59.2%	59.3%

ATPC: 75%		*0*	*5*	*10*	*15*	*20*	*25*	*FM–RFM*
	0	51.5%	56.1%	59.7%	62.2%	63.9%	64.8%	65.5%
	2	51.5%	56.2%	60.2%	63.3%	65.1%	66.0%	66.7%
RFM (dB)	*4*	51.5%	56.4%	60.4%	63.6%	65.4%	66.2%	66.7%
	6	51.5%	56.5%	60.6%	63.5%	65.1%	65.8%	66.3%
	8	51.5%	56.5%	60.4%	63.1%	64.4%	65.1%	65.4%
	10	51.4%	56.3%	59.9%	62.3%	63.4%	63.8%	64.1%

ATPC: 100%		*0*	*5*	*10*	*15*	*20*	*25*	*FM–RFM*
	0	51.5%	58.0%	64.2%	69.2%	73.3%	75.9%	77.9%
	2	51.5%	58.3%	64.8%	70.2%	74.1%	76.1%	77.6%
RFM (dB)	*4*	51.5%	58.5%	65.0%	70.3%	73.7%	75.4%	76.5%
	6	51.5%	58.7%	65.0%	69.8%	72.7%	74.0%	74.9%
	8	51.5%	58.6%	64.7%	68.9%	71.2%	72.2%	72.9%
	10	51.4%	58.3%	63.7%	67.3%	69.2%	69.9%	70.4%

50–60% **60–70%** **70–80%**

Figure 36: Variation of assignments to channel 1

[9] The results for an ATPC range of 'FM – RFM' assume, in effect, ideal ATPC equipment that is able to change its EIRP to cover the fade margin, no matter how large (or small) the fade margin happens to be for a particular link. An RFM of 0 dB is not realistic, but is included as a limiting case.

ATPC Range (dB)

ATPC: 0%	RFM (dB)	0	5	10	15	20	25	FM–RFM
	0	294	294	294	294	294	294	294
	2	294	294	294	294	294	294	294
	4	294	294	294	294	294	294	294
	6	294	294	294	294	294	294	294
	8	294	294	294	294	294	294	294
	10	294	294	294	294	294	294	294

ATPC: 25%	RFM (dB)	0	5	10	15	20	25	FM–RFM
	0	294	280	280	266	266	266	266
	2	294	280	266	266	266	266	266
	4	294	280	266	266	266	266	266
	6	294	280	266	266	266	266	266
	8	294	280	266	266	266	266	266
	10	294	280	266	266	266	266	266

ATPC: 50%	RFM (dB)	0	5	10	15	20	25	FM–RFM
	0	294	287	266	266	273	266	266
	2	294	287	266	252	266	266	266
	4	294	287	266	266	266	266	266
	6	294	287	266	252	252	252	252
	8	294	287	266	252	252	252	252
	10	294	287	266	252	252	252	252

ATPC: 75%	RFM (dB)	0	5	10	15	20	25	FM–RFM
	0	294	266	266	224	245	224	224
	2	294	266	266	238	224	210	210
	4	294	266	266	238	224	210	210
	6	294	266	266	238	224	210	210
	8	294	266	266	238	231	217	217
	10	294	266	266	238	217	217	217

ATPC: 100%	RFM (dB)	0	5	10	15	20	25	FM–RFM
	0	294	266	210	196	168	168	168
	2	294	266	210	182	168	168	168
	4	294	266	210	182	168	168	168
	6	294	266	238	210	196	196	196
	8	294	266	224	210	196	196	196
	10	294	266	224	210	210	196	196

300–250 MHz **250–200 MHz** **200–150 MHz**

Figure 37: Variation of maximum bandwidth

4.1.3 Clash test excesses

The automated planning process is based on the iterative assessment of link compatibility. In the terminology of the propagation library used[10] these compatibility tests are 'clash' tests. As each new assignment is made, clash tests are calculated with all existing assignments within the co-ordination zone (70 km). The clash test calculates a numerical 'excess' value: if the excess is negative, then the link is compatible; if the excess is positive then the required W/U ratio is not satisfied (i.e. an assignment is not possible for that channel). Figure 38 shows a cumulative distribution function of clash test excesses for a non-ATPC and an ATPC plan: it is apparent that in an automated, efficient plan a significant proportion of interfering paths will have relatively small negative excesses (i.e. may potentially cause interference)[11].

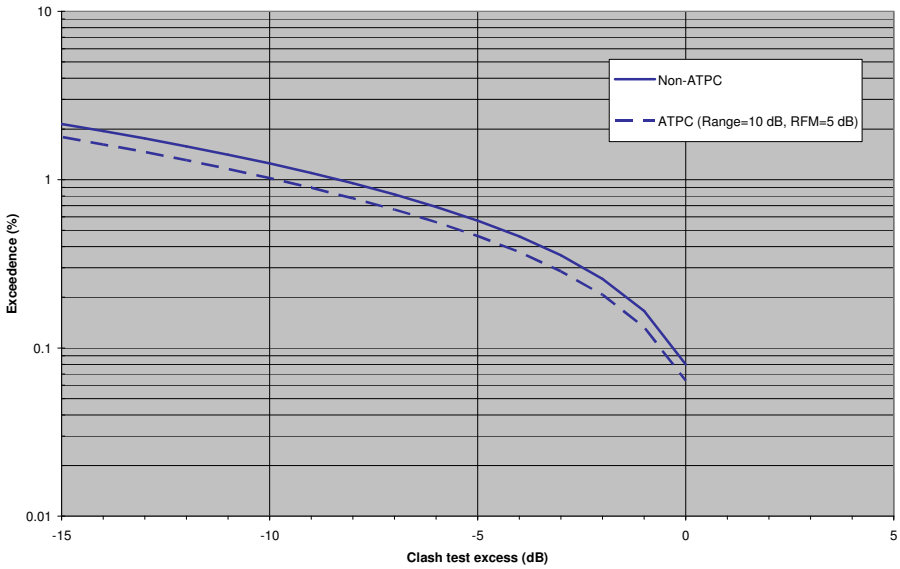

Figure 38: CDF of clash test excesses

4.2 Analysis tool

The analysis tool takes a plan generated by the planning tool (or by another process) and applies a sequence of rain fields, evaluating system performance as measured by outage probabilities. For each rain field, the fade on each link is calculated, which then allows the EIRP uplift to be determined for each ATPC link. Every link is then tested in turn against all interfering paths, for all rain fields, and the number of outages recorded (distinguishing between those outages directly caused by a rain fade and those outages caused by ATPC-enhanced interference); the ATPC-induced outage counts reported here are 'extra' outages (i.e. those outages occurring in a link that is not also in outage because of a rain fade that exceeds its fade margin).

4.2.1 Area to be simulated

The rain fields with measured rainfall rates are 56.4 km square (188 pixels of 300 m). In order to avoid edge effects, the analysis of link performance is not performed on the whole area, but on a smaller 'test' area; interference, however, is considered from links throughout the entire

[10] Propagation calculations are based on Ofcom's MWM library.

[11] By definition, a planned set of links will have no interfering paths whose clash test excess exceeds 0 dB. In a plan with ATPC links, the effect of rain fades will be to cause some excesses to become more positive as the ATPC increases EIRP on the interfering link—the simulator then records an ATPC-induced outage whenever an excess becomes positive (taking into account the state of the wanted signal).

area (the 'background'). Initial simulations were run using a square 25 km test area set in the centre of the 56.4 km background area, but analysis of the lengths of interfering paths showed that this was rather conservative: more links could be analysed if the size of the test area were to be increased, and the results presented here are for a test area of 35 km (see section 4.2.6 for more detail).

The simulated rain fields had somewhat larger area coverage, which allowed the test area size to be increased to include more links. Simulations were run with a test area of 35 km (background 56.4 km) and 50 km (background 70 km). The pixel size for the simulated rain data was 100 m.

The 38 GHz fixed link database was processed to determine the number of links it would be possible to include in the analysis, and to determine where to locate the area centre point. An indication of the number of links in areas of various sizes is shown in the following table.

Size of Square	Maximum Links
25 x 25 km	1,172
50 x 50 km	2,117
75 x 75 km	2,859
100 x 100 km	3,473
125 x 125 km	4,006
150 x 150 km	4,594
175 x 175 km	5,272
200 x 200 km	6,086

Table 6: Number of links available

Link density across the UK is shown in figure 39, for an assumed area size of 50 km. The centre point for the analyses presented here was chosen as the maximum of the 25 km distribution, which is at TQ340760[12].

[12] For comparison, simulations were also performed for two other maxima in the link density distribution: 'Birmingham' at SP020900 and 'Manchester' at SD820000. However, no systematic differences were found in comparison with the London results.

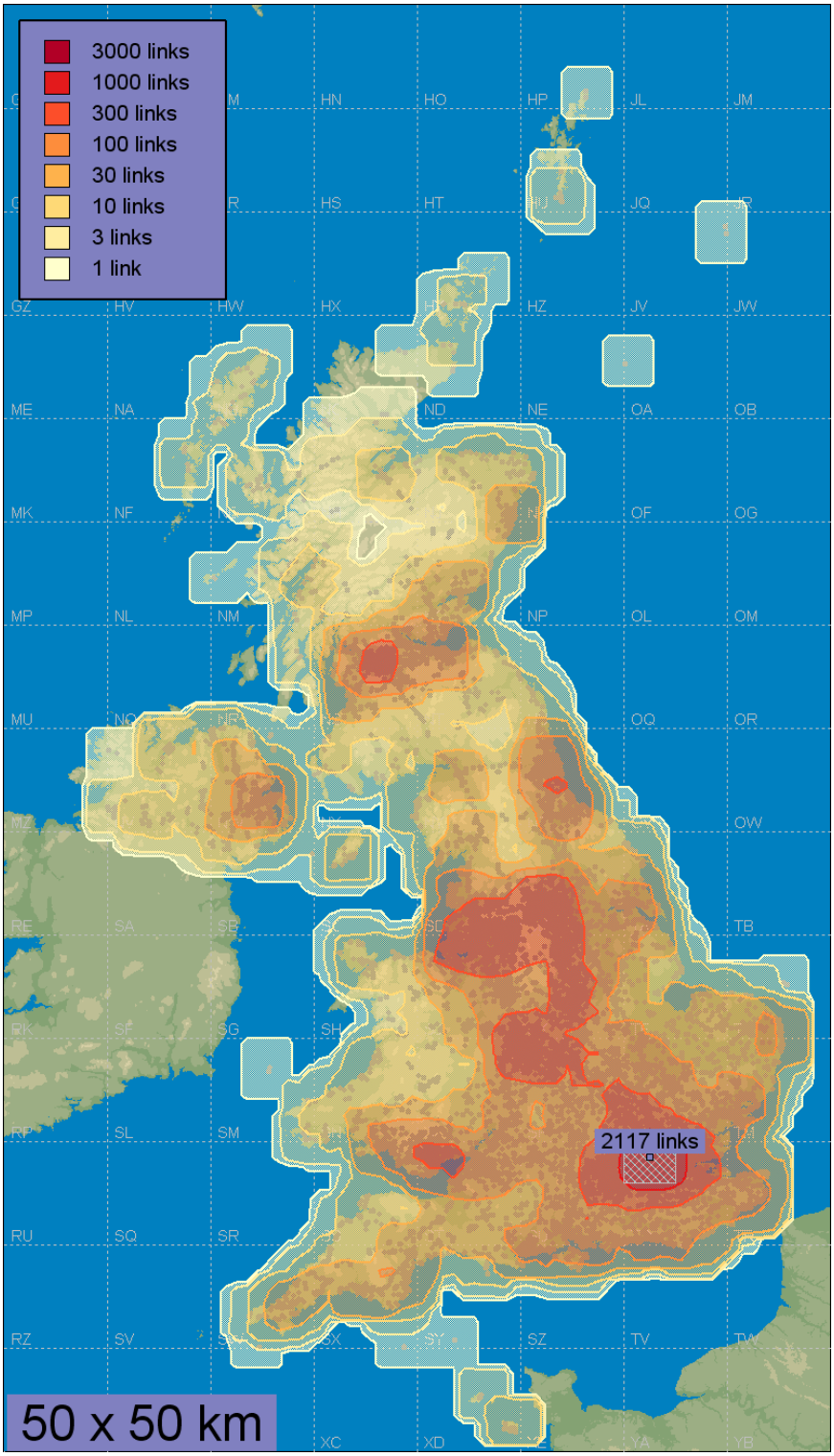

Figure 39: Link density in the 38 GHz band

4.2.2 Results of rain analysis

The number of detected outages will depend upon the severity and distribution of the rain. Three types of measured rain data were used (convective, stratiform and frontal), as well as two types of simulated rain data (convective and stratiform)[13]. The maximum rainfall rates for the measured convective, stratiform and frontal rain data were 52.5, 45.7 and 95.5 mm/hr respectively[14]. The simulated rain data was scaled to 45 mm/hr for convective and 30 mm/hr for stratiform. The distribution of rainfall rate and fades can be seen in figures 40a and 40b.

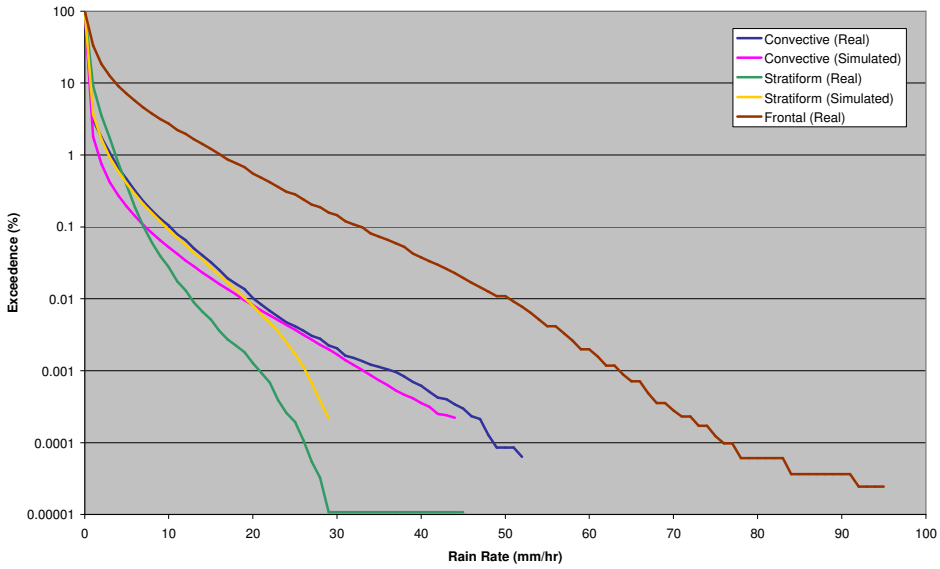

Figure 40a: Rainfall rate for various rain types

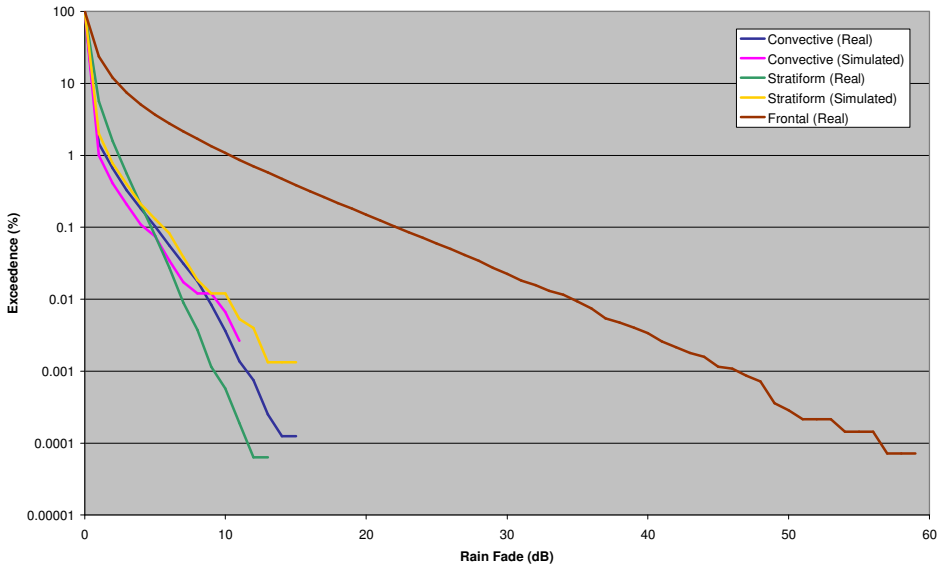

Figure 40b: Rain fades for various rain types

[13] The measured rain data forms a sequence of rain fields in which a clear time progression is apparent, whereas each field in the simulated sequence is independent and time is not a consideration.

[14] It is evident from figure 40a that the maximum rainfall rate for the measured stratiform event is somewhat misleading: the effective maximum is ~30 mm/hr, which is the same as the simulated data.

The rain will directly cause an outage in a link if the fade exceeds the link's fade margin (whether or not the link uses ATPC)—in other words, when the 'signal excess' (*fade–FM*) exceeds 0 dB. The following figure shows the distribution of signal excess for each of the rain types, and for simulations with and without ATPC. It is clear from the results that the convective and stratiform rain will not directly cause any significant number of outages[15], whereas the frontal rain will cause a significant number of outages[16].

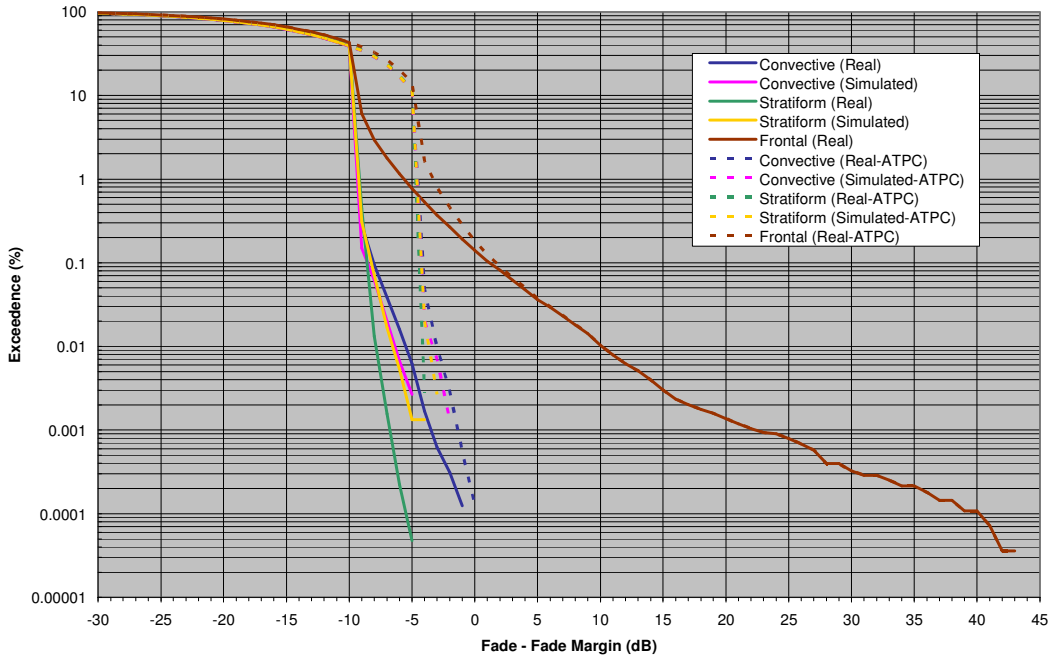

Figure 40c: 'Signal excess' for various rain types

The effect of introducing ATPC is apparent in figure 41, in which the number of extra, ATPC-induced outages rises as the proportion of ATPC links increases[17]; in the example shown, the number of extra outages is 12% of the total. The number of outages directly caused by rain also increases with ATPC penetration, even though ATPC does not, in itself, reduce the protection a link has against rain fading: this rise is caused by the progressive withdrawal of 'excessive' fade margin as non-ATPC links with the 10 dB minimum fade margin are replaced by ATPC links with a lower fade margin (e.g. an RFM of 5 dB); if the remote fade margin is increased to 10 dB, the number of direct outages then remains constant as the ATPC penetration increases (in figure 41, see the curve for an ATPC range of 20 dB and an RFM of 10 dB). The results also show the trade-off introduced by assumptions about ATPC equipment capability: a larger ATPC range results in a more efficient plan (see figures 36 and 37) because EIRPs are minimised; however, if the ATPC range is smaller than typical *FM–RFM* values then some links will have 'excessive' RFM—and will be better protected against interference (e.g. if the fade margin for a link is 25 dB and the ATPC range is 10 dB, then the link will operate at *25 dB – 10 dB = 15 dB* above RSL, even if the required RFM is only 5 dB). Matching the ATPC range and remote fade

[15] The measured convective rain data set does in fact cause four outages for the ATPC plan considered here (ATPC range = 10 dB, RFM = 5 dB).

[16] The 'cliff edge' effect at –10 dB in the non-ATPC cases is caused by the minimum fade margin policy for the band; a similar effect is also apparent at –5 dB for the ATPC cases, corresponding to the remote fade margin (which acts as an effective minimum).

[17] The graph plots the number of outages, rather than the percentage, to avoid mistakenly interpreting the results as annual statistics—the probability of each rain event is not known and the results cannot therefore be compared directly with planned unavailability.

margin appears to be a very effective method of reducing ATPC-induced outages (see the curve for an ATPC range of 10 dB and an RFM of 10 dB).

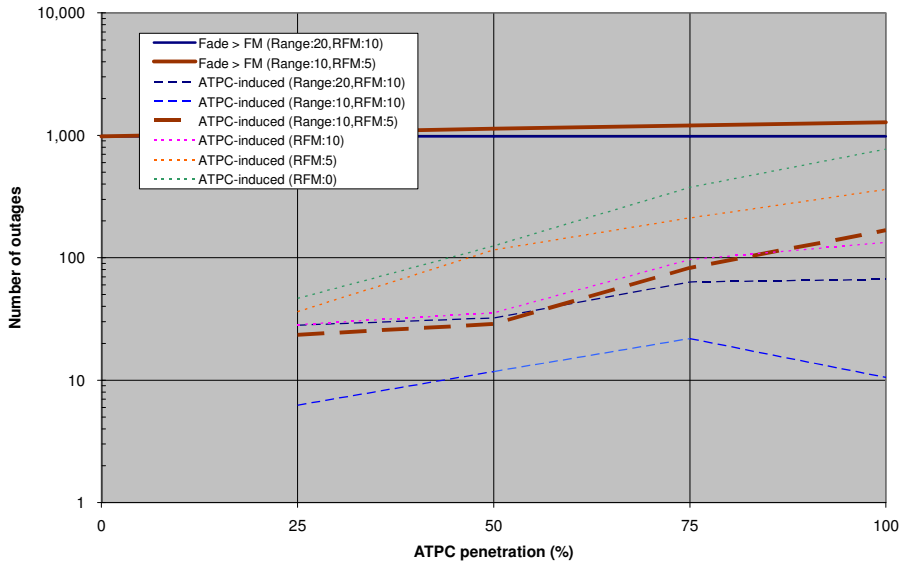

Figure 41: Number of extra outages

4.2.3 Effect of correlation in the rain field

Figure 41 shows the effect of testing an automated plan with measured rain fields, and the resulting ATPC-induced outages. Depending on the characteristic spatial distribution of the rain, an aggravating factor causing these outages is the correlation between power increases on the interfering link with fading on the victim link; however, a mitigating factor is expected to be the presence of correlation between the rain fades on the interfering and victim links and rain fading along the interfering path. A brief investigation has been performed to illustrate the extent of this mitigation, by suppressing the rain fades on all interfering paths and noting the increase in the number of ATPC-induced outages. These results are shown in figure 42.

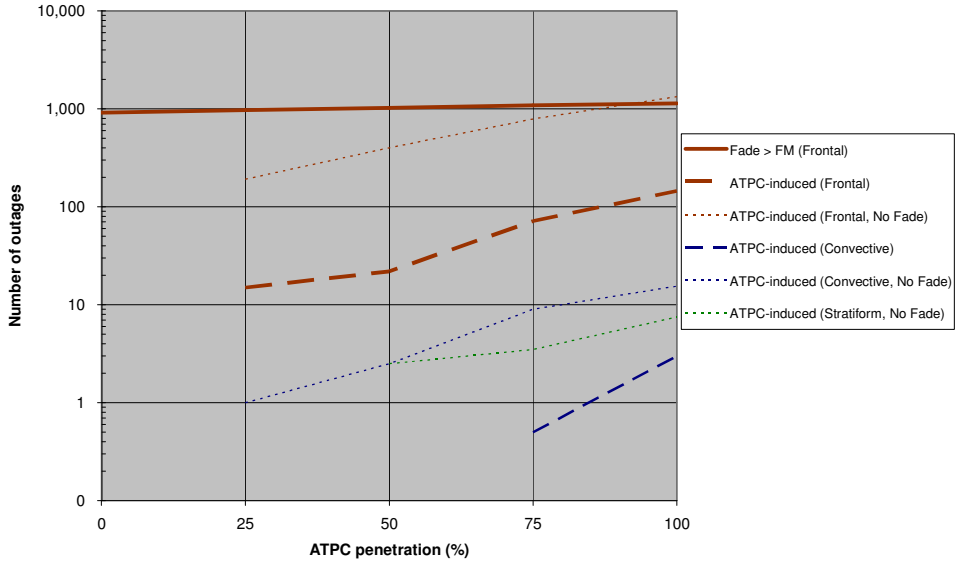

Figure 42: Mitigating effect of interfering path fades

When the rain fades on interfering paths are artificially removed, then the number of ATPC-induced outages increases dramatically: for the frontal rain event, the number of extra outages actually exceeds the number of direct outages in the all-ATPC case, and outages are now present in the relatively less intense convective and stratiform rain events. It is clear from this limiting case that correlated fading on the interfering path acts as a significant mitigating factor for ATPC-induced outages.

4.2.4 Mitigation of ATPC-induced outages

It has been shown earlier that improvements in band efficiency result from the introduction of ATPC, but that additional outages then occur (during intense rain). The question then arises of whether changes to the planning process could be made that retain the efficiency gains but reduce the number of ATPC-induced outages. Three such adjustments have been investigated:

1. Increasing the fade margin for all links.
2. Increasing (or decreasing) the required W/U ratios for all links.
3. Increasing the interference margin.

The effect of increasing the fade margin (i.e. EIRP) of all links is shown in the following figures, where it is apparent that the method is not effective: as expected, the band efficiency is reduced somewhat, but without reducing the number of ATPC-induced outages. As the fade margins increase the total number of outages decreases because of the extra protection against direct rain outages, but those links affected by a nearby ATPC link receive no specific protection[18].

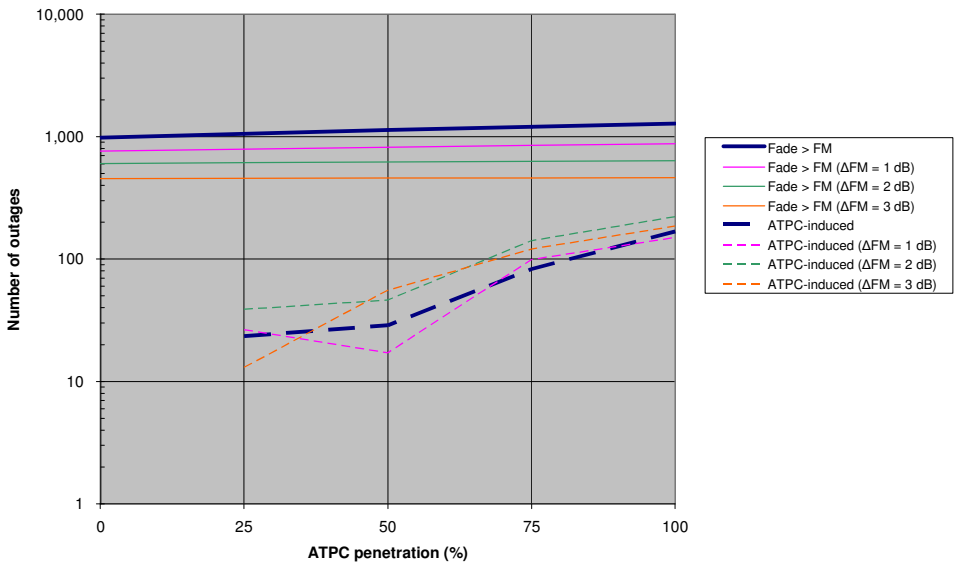

Figure 43: Effect of increasing fade margin on outages (frontal event)

[18] An increase of 1 dB in fade margin 'cancels' the extra outages caused by ATPC during the frontal rain event (for an ATPC range of 10 dB and an RFM of 5 dB).

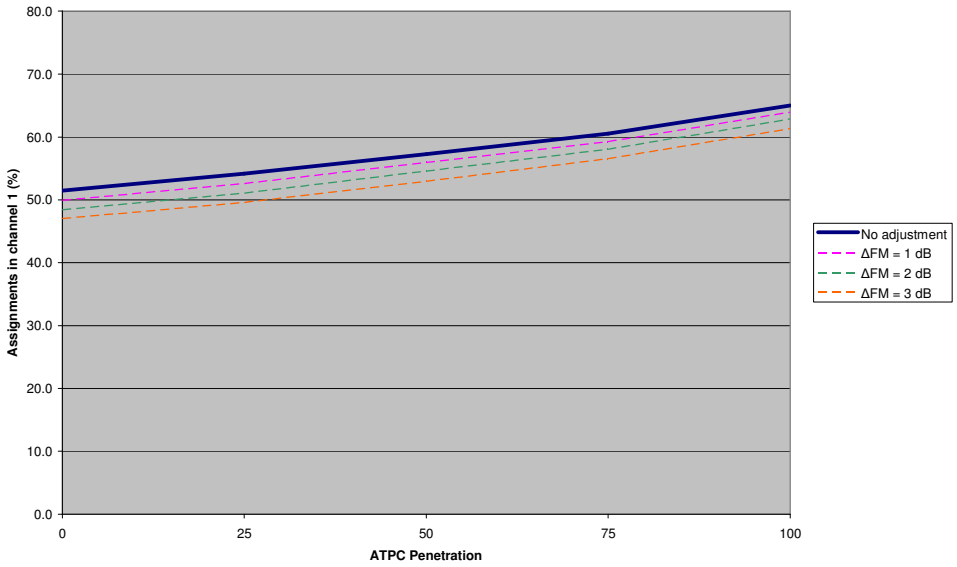

Figure 44: Effect of increasing fade margin on efficiency

The second mitigation approach was to vary the W/U ratios used in planning, in the expectation that this would specifically provide extra protection against interference. The results are shown in figures 45–47. Adjusting the W/U ratios in the planning process and then using the same adjusted values to judge whether an outage occurs in the rain analysis produces the paradoxical result that increasing the W/U ratios actually increases, not decreases, the number of outages (see figure 45). The explanation for this is seen in figure 38—in a relatively efficient plan, there will always be a large number of interfering paths with small clash test excesses, 'ready' to cause interference. Band efficiency, however, behaves as expected—increasing the required W/U results in a relatively less efficient plan; decreasing the required W/U results in a relatively more efficient plan.

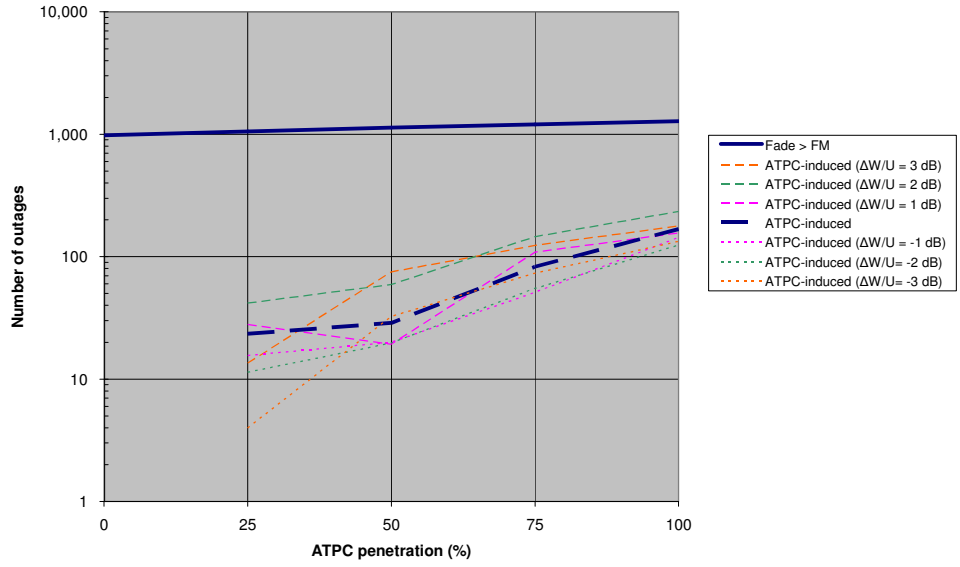

Figure 45: Effect of adjusting W/U criteria on outages (frontal only)

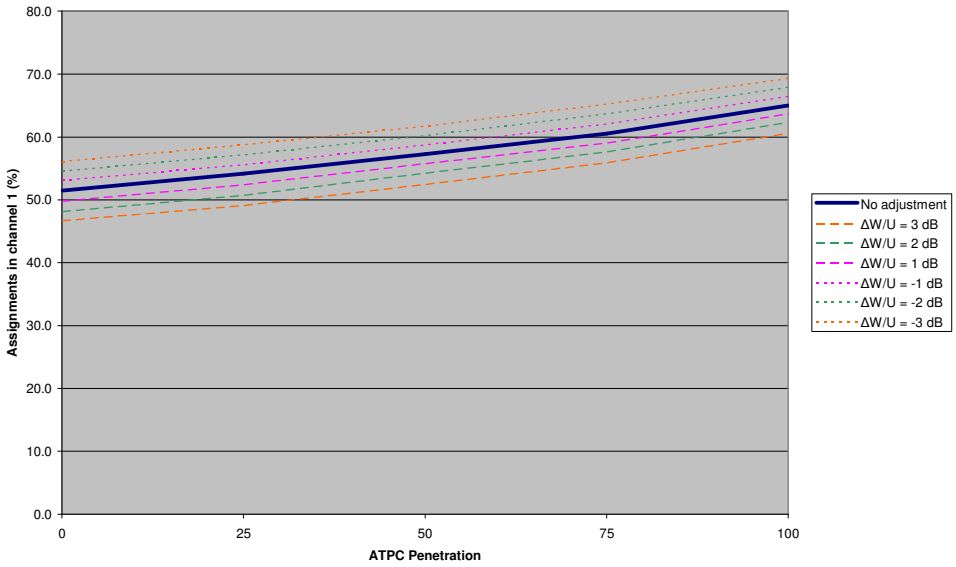

Figure 46: Effect of adjusting W/U criteria on efficiency

In practice, a better definition of a simulated outage might be to adjust W/U when planning, but to assume the original W/U values when performing the rain analysis. The results are then as expected: increasing W/U now removes some, but not all, of the ATPC-induced outages; similarly, reducing the W/U protection increases outages. Note that adjusting W/U, while leaving RSL unchanged, has no effect on the number of direct outages.

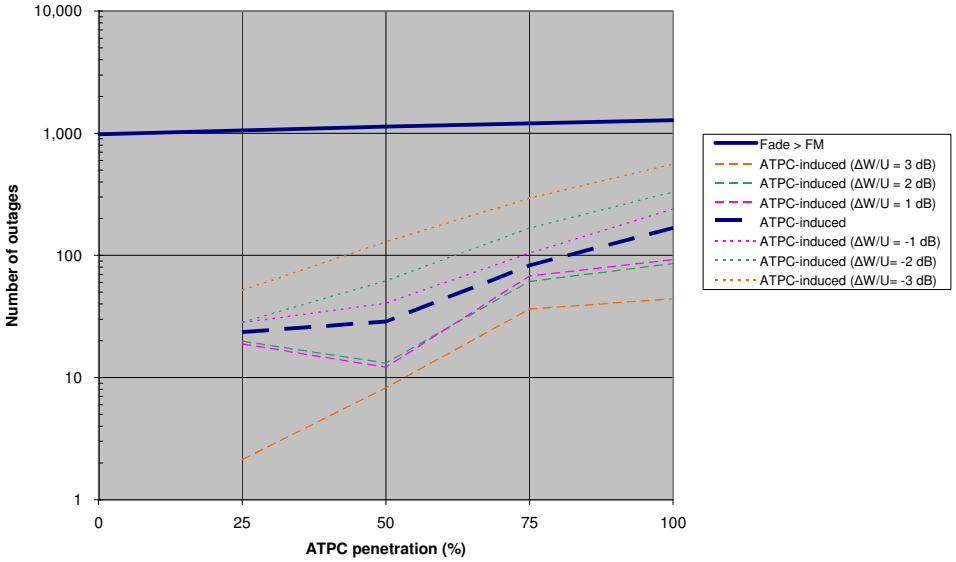

Figure 47: Effect of adjusting W/U criteria on outages (frontal only)

The final approach is to adjust the interference margin. The results are shown in figures 48–49. As expected, increasing the interference margin increases efficiency (though with diminishing effect), whereas there is effectively no change in the number of ATPC-induced outages.

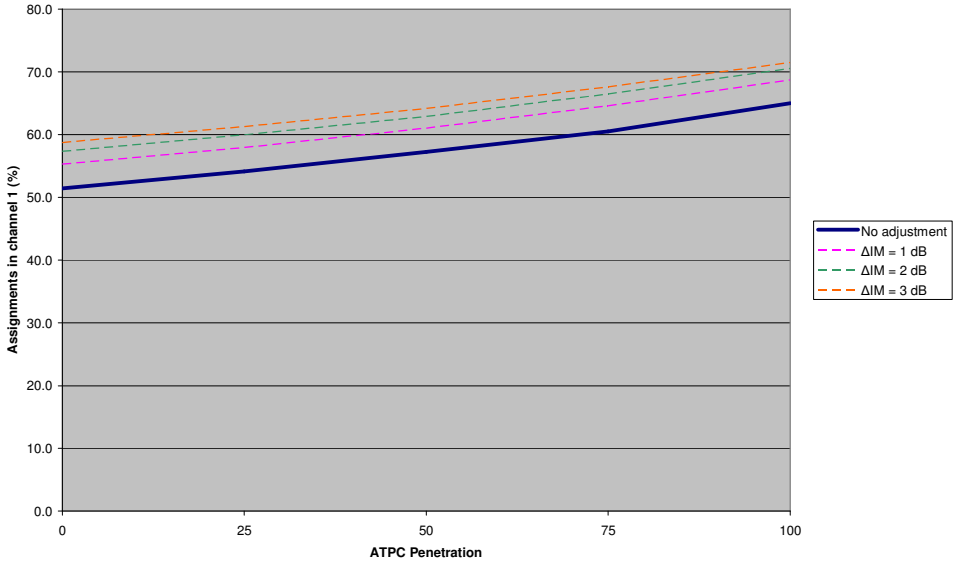

Figure 48: Effect of adjusting interference margin on efficiency

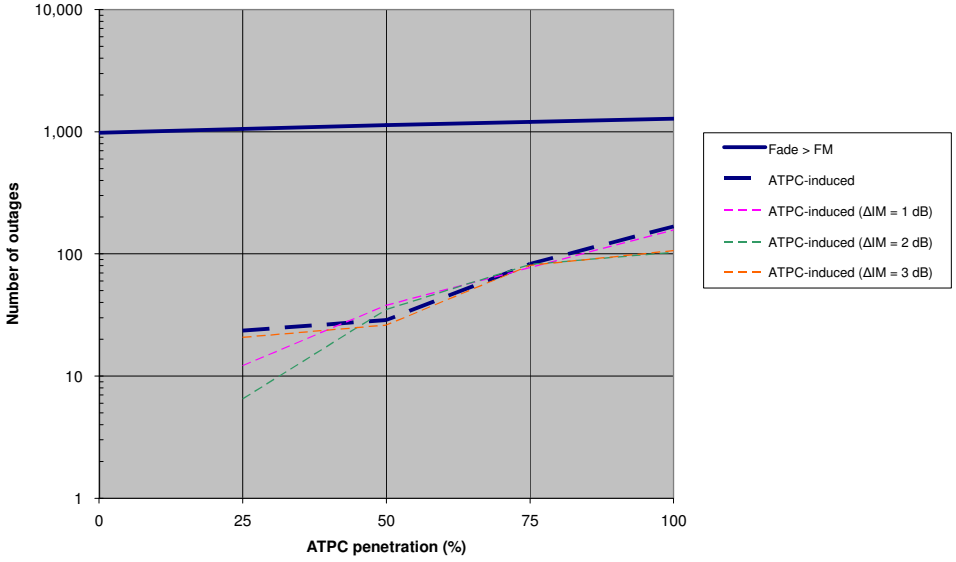

Figure 49: Effect of adjusting interference margin on outages (frontal only)

In summary, adjusting W/U in the planning process is a more effective technique for reducing ATPC-induced outages than adjusting the fade margins or interference margin. However, it is evident that none of these band-wide mitigation techniques targets the ATPC-induced outages very effectively.

4.2.5 Example outage event

An example outage event is shown in figure 50. Three variables are plotted for each of the 231 rain fields in the frontal sequence (with two supplementary variables):

- *Interfering Link.* The change in EIRP on the interfering link. The interfering path is very short in this example and the correspondence between EIRP increases on the interfering link and fading on the wanted link is very close. A second variable shows the change in EIRP including the effect of rain fading on the interfering path: however, there is no significant fading on this particular interfering path.
- *Wanted Link.* The 'signal excess' (*fade–FM*); a second variable shows the effective signal excess, taking into account the effect of ATPC. When the signal excess becomes positive, then the wanted link is in outage.
- *Wanted Link and Interfering Link.* The clash test excess. When the clash test excess becomes positive, then the wanted link has an interference-induced outage. Note that the second outage (at sequence number 66) is not an 'extra' outage, as the clash test excess and the signal excess are both positive.

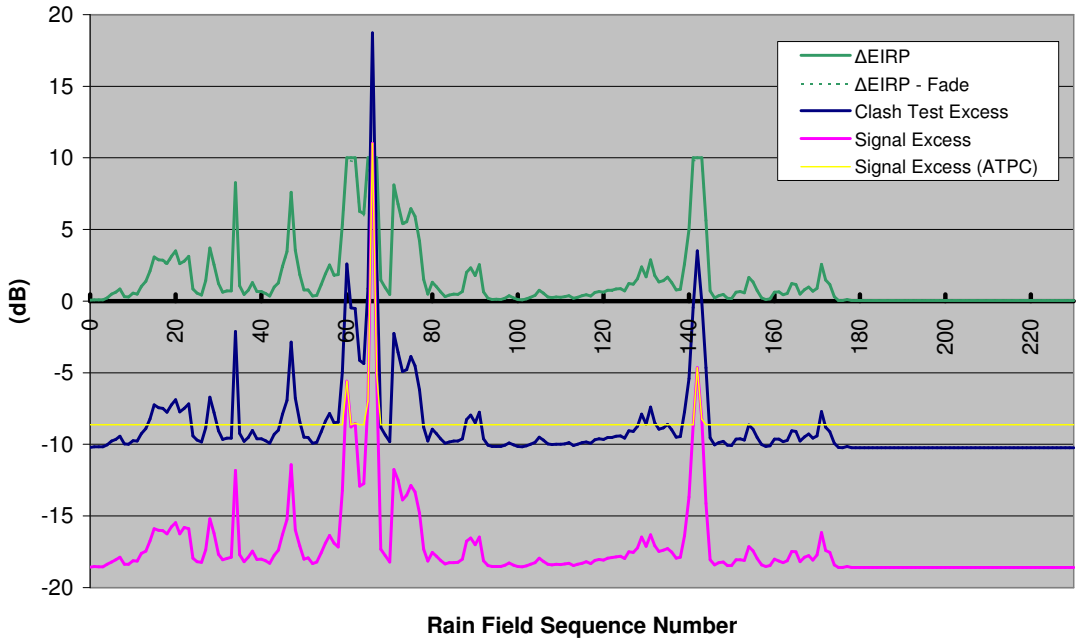

Figure 50: Trace of simulated excesses for a single link

4.2.6 Interfering path lengths

Link performance in the presence of rain was assessed for a square area centrally located within the supplied rain fields, with a buffer zone to prevent edge effects: the size of this buffer zone was determined iteratively by examining the lengths of those interfering paths that caused outages. A typical CDF is shown in figure 51, which supports the choice of a 35 km test area within the 56.4 km background area (i.e. a buffer zone width of 10.7 km). The distribution also shows a significant number of short, possibly spurious, paths: parallel links are excluded from the analysis (i.e. links for which each end is within 2 m horizontally and 10 m vertically); mast sharing was determined by co-ordinate equality—no attempt was made to aggregate locations.

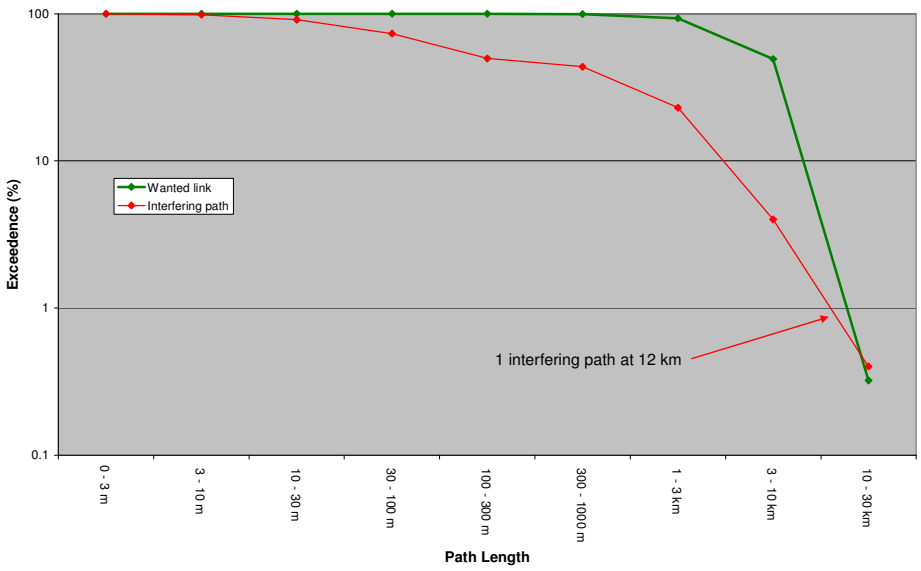

Figure 51: Distribution of path lengths

5. Application of ATPC to other bands above 18 GHz

The gain in band efficiency resulting from the introduction of ATPC derives from the reduction in planned EIRP for ATPC links, in which the EIRP is reduced by the difference between the fade margin and the remote fade margin. Remote fade margins are typically in the range 3–7 dB and are not frequency dependent; the mean calculated fade margin for the 38 GHz band is approximately 19 dB, which is similar to the values for other high frequency bands—ATPC should therefore be equally applicable in these bands.

The following table gives fade margin statistics for UK fixed link bands.

Band	Mean Fade Margin	Mode[19]
13 GHz	15.8 dB	15 dB
15 GHz	18.9 dB	10 dB
18 GHz	12.3 dB	10 dB
23 GHz	20.3 dB	10 dB
25 GHz	21.9 dB	10 dB
38 GHz	17.9 dB[20]	10 dB

Table 7: Fixed link fade margins

For frequencies above 60 GHz, results from the final report for the SES project "Reliable radio communications at frequencies of 60 GHz and above" [Ventouras et al, 2005] suggest that ATPC has the potential to improve spectrum efficiency in bands above 60 GHz. Simulation work carried out at these frequencies shows that the clear-sky case (with no rain attenuation) is the worst case for frequencies above 60 GHz, i.e. a worse W/U is predicted in clear sky than in rain. Hence, designing a link to clear-sky specifications

[19] The minimum fade margin is the most frequently assigned value.
[20] When re-planned using the automated tool developed for this study, the mean fade margin was 19.3 dB.

and compensating for rain fading dynamically on a dB by dB basis will minimise the separation distance between the links.

6. Conclusions

The following conclusions have been identified by this study:

1. The spatial autocorrelation function of rain fields falls off approximately exponentially with distance. A fractal model has been used to simulate rain fields used in the analysis programme. The simulator is capable of producing stratiform-like and convective-like synthetic rain fields, with fractal dimension of contour lines enclosing areas of rain greater than or equal to a threshold, and a spectral density function exponent and spatial autocorrelation function consistent with measured data.

2. The implementation of ATPC in the 38 GHz band gives significant improvements in spectrum efficiency as measured by the increase in the number of links assigned to channel 1 (from ~50% to ~70%) and the decrease in the maximum bandwidth used (from ~300 MHz to ~180 MHz). The introduction of ATPC does give rise to a number of additional outages in the presence of intense rain (~10% increase in frontal rain). These additional outages can be mitigated to some extent by band-wide changes to the planning process and by matching the ATPC range with the remote fade margin; however, the outages cannot be wholly eliminated by the methods examined here.

3. Adjusting W/U in the planning process is a more effective technique for reducing ATPC-induced outages than adjusting the fade margins or interference margin. However, it is evident that none of these band-wide mitigation techniques targets the ATPC-induced outages very effectively.

4. Based on the similarity of average fade margins between the 38 GHz band and other high frequency fixed link bands, gains in spectrum efficiency should equally be possible in those other bands.

7. References

Bacon, D. “Rain Modelling and the Future of Telecommunications” Rainmap Kick-off conference, London, 12th January 2005 (http://www.rainmap.rl.ac.uk)

Barbaliscia, F., Ravaioli, G., Paraboni, A., “Characteristics of the spatial statistical dependence of rainfall rate over large areas” IEEE Trans. on Ant. and Prop., vol. 40, n.1, pp8–12, 1992

Callaghan, S.A., “Fractal analysis and synthesis of rain fields for communication systems design” PhD thesis, University of Portsmouth, 2004

Charles, S.P., Bates, B.C., Hughes, J.P. “A spatiotemporal model for downscaling precipitation occurrence and amounts”. Jnl. Geophys. Res., Vol. 104, D24, December 1999

Cowpertwait P. S. P., “A Generalized Spatial-Temporal Model of Rainfall Based on a Clustered Point Process”, Proc. R. Soc. Lond. A,, Vol. 450, no. 1938, pp. 163–175, 1995.

Cox, D., Isham, V., “A simple spatial-temporal model of rainfall” Proc. R. Soc. Lond. A415 317–328, 1988

Deidda, R., “Multifractal analysis and simulation of rainfall fields in space”, Physics and Chemistry of the Earth Part B—Hydrology, Oceans and Atmosphere, 24 (1-2), 73–78, 1999

Enjamio, C., Vilar, E., Fontan, F.P. and Redaño, A., “Rainfall Rate Spatial Distribution at Local Scale: Raincell Analysis in the Mediterranean Region”, URSI Open Symposium on Propagation and Remote Sensing, Garmisch-Partenkirchen, Germany, 12th to 15th February 2002.

Feder, J., “Fractals”, Plenum Press, 1988

Gremont, B., “Simulation of Rainfield Attenuation for Satellite Communication Networks.” COST 280 First International Workshop on *Propagation Impairment Mitigation for Millimetre Wave Radio Systems,* Qinetiq, Malvern, July 2002 (available from http://www.cost280.rl.ac.uk/)

Handbook on Digital Radio-Relay Systems (ITU-R, 1996)

Koutsoyiannis, D., Onof, C., “Rainfall disaggregation using adjusting procedures on a Poisson cluster model”, Journal of Hydrology, 246, 109–122, 2001

Kraichnan R. H. and Montgomery, D. "Two dimensional turbulence," Rep. Prog. Phys., Vol. 43, pp. 547–619, 1980.

Lewis, J.P. “Generalized stochastic subdivision” ACM Transactions on Graphics Vol. 6 No 3 July 1987.

Mandelbrot, B.B., “The fractal geometry of nature”, San Francisco, CA, Freeman, 1983

Marsan, D., Schertzer, D., Lovejoy, S., “Causal space-time multifractal processes: predictability and forecasting of rain fields”, Jnl. Geophys. Res., Vol. 101, D21, Nov. 1996

National Spectrum Managers Association Working Group 18 Recommendation on Adaptive Power Control (WG18-91-032)

Onof, C., Northrop, P., Wheater, H., Isham, V., “Spatiotemporal storm structure and scaling property analysis for modeling”, Jnl. Geophys. Res. Vol. 101, D21, 26,415–26,425, 1996

Over, T.M., and Gupta, V.K., “A space-time theory of mesoscale rainfall using random cascades”, Jnl. Geophys. Res., Vol 101, D21, 26,319–26,331, 1996

Paraboni, A., Masini, G., Riva, C., “The spatial structure of rain and its impact on the design of advanced TLC systems” pp.169–172, Proc. Fourth Ka Band Utilization Conf. Venice, Italy, Nov 2–4, 1998

Paulson, K.S., “The spatial temporal statistics of rain rate random fields”, Radio Science, 37(5) 2002

Richardson, K.W., Thomas, D.W., Callaghan, S.A., Gremont, B. “Study to assess the impact of fade mitigation techniques in bands above 20 GHz: Final report”. Project report for Ofcom, 2004

Tessier, Y., Lovejoy, S., Schertzer, D., “Universal mulitfractals—theory and observations for rain and clouds”, Jnl. Appl. Meteorol. 32(2), 22–150, 1993

Ventouras, S. et al, “Reliable radio communications at frequencies of 60GHz and above” Final report for Ofcom, December 2005.

Voss, R. F., "Random fractal forgeries", in *Fundamental Algorithms for Computer Graphics*, editor R. A. Earnshaw, NATO ASI Series F, Computer and System Sciences, Vol 17, 1985

Wheater, H.S., Isham, V.S., Cox,D.R., Chandler,R.E., Kakou,A., Northrop, P.J., Oh, L., Onof, C., Rodriguez-Iturbe, I., "Spatial-temporal rainfall fields: modelling and statistical aspects", Hydrology and Earth Systems Sciences, 4(4), 581–601, 2000

Appendix 1: Spectral modelling of random processes

Gaussian processes are commonly adopted as a computationally tractable, yet reasonably powerful, class of stochastic model [Lewis, 1987], with parameters mean $\mu_{01} = \mu_{10} = E\{x\}$ and variance $\mu_{02} = \mu_{20} = E\{x^2\}$, where $E\{x\}$ is the expectation.

The *autocorrelation function* is given by:

$$\mu_{11} = R(\tau) = E\{x(t)x(t+\tau)\} = \int\int x_1 x_2 dF_x(x_1, x_2; t, t+\tau)$$

For a stationary process:

- $R(\tau) = R(-\tau)$
- $R(0) \geq | R(\tau) |$
- $R(x) = E\{x^2\}$

It is assumed that all processes are normalized to have zero mean and unit variance.

Intuitively, the autocorrelation function describes the correlation between a random function and a copy of itself shifted by some distance ("lag"). For example, a completely uncorrelated or "white" noise has an autocorrelation function $\delta(0)$ (Dirac impulse function), while a constant signal is equally correlated with itself at all lags and so has $R(\tau) = 1$ .Usually the autocorrelation function decreases continuously away from the origin, corresponding to a noise that is neither completely uncorrelated nor deterministic. The autocorrelation function of a noise with an oscillatory character includes an oscillatory component that is damped away from the origin; the period of this component corresponds to the average period of the oscillation in the noise while the amount of damping is related to the spectral bandwidth and the irregularity of the oscillation in the noise.

Stochastic modeling using Gaussian statistics and the second-order moments may be termed *spectral modeling* since the noise autocorrelation function and power spectrum specify equivalent information, and in fact are a Fourier transform pair (Wiener-Khinchine relation):

$$S(\omega) = \int_{-\infty}^{\infty} R(\tau) \exp(-j\omega\tau) d\tau$$

Since the power spectrum is by definition nonnegative, the Wiener-Khinchine relation requires that (physically meaningful)autocorrelation functions be *non-negative definite*. This condition will be important in selecting functions to be used as autocorrelations. As an intuitive example of the existence of constraints on the autocorrelation function, we would expect by transitivity that if a noise is highly correlated with itself at a particular lag, it should also show correlation at multiples of that lag.